Laser altimetry reveals complex pattern of Greenland Ice Sheet dynamics

Beata M. Csatho[a,1], Anton F. Schenk[a], Cornelis J. van der Veen[b], Gregory Babonis[a], Kyle Duncan[a], Soroush Rezvanbehbahani[c], Michiel R. van den Broeke[d], Sebastian B. Simonsen[e], Sudhagar Nagarajan[f], and Jan H. van Angelen[d]

[a]Department of Geology, University at Buffalo, Buffalo, NY 14260; Departments of [b]Geography and [c]Geology, University of Kansas, Lawrence, KS 66045; [d]Institute for Marine and Atmospheric Research, Utrecht University, 3584 CC Utrecht, The Netherlands; [e]Division of Geodynamics, DTU Space, National Space institute, DK-2800 Kgs. Lyngby, Denmark; and [f]Department of Civil, Environmental and Geomatics Engineering, Florida Atlantic University, Boca Raton, FL 33431

Edited* by Ellen S. Mosley-Thompson, The Ohio State University, Columbus, OH, and approved November 17, 2014 (received for review June 23, 2014)

We present a new record of ice thickness change, reconstructed at nearly 100,000 sites on the Greenland Ice Sheet (GrIS) from laser altimetry measurements spanning the period 1993–2012, partitioned into changes due to surface mass balance (SMB) and ice dynamics. We estimate a mean annual GrIS mass loss of 243 ± 18 Gt·y^{-1}, equivalent to 0.68 mm·y^{-1} sea level rise (SLR) for 2003–2009. Dynamic thinning contributed 48%, with the largest rates occurring in 2004–2006, followed by a gradual decrease balanced by accelerating SMB loss. The spatial pattern of dynamic mass loss changed over this time as dynamic thinning rapidly decreased in southeast Greenland but slowly increased in the southwest, north, and northeast regions. Most outlet glaciers have been thinning during the last two decades, interrupted by episodes of decreasing thinning or even thickening. Dynamics of the major outlet glaciers dominated the mass loss from larger drainage basins, and simultaneous changes over distances up to 500 km are detected, indicating climate control. However, the intricate spatiotemporal pattern of dynamic thickness change suggests that, regardless of the forcing responsible for initial glacier acceleration and thinning, the response of individual glaciers is modulated by local conditions. Recent projections of dynamic contributions from the entire GrIS to SLR have been based on the extrapolation of four major outlet glaciers. Considering the observed complexity, we question how well these four glaciers represent all of Greenland's outlet glaciers.

Greenland Ice Sheet | laser altimetry | mass balance | ice dynamics

Comprehensive monitoring of the Greenland Ice Sheet (GrIS) by satellite observations has revealed increasing mass loss since the late 1990s (1, 2), reaching 263 ± 30 Gt·y^{-1} for the period 2005–2010 (3). This translates to a sea level rise (SLR) of 0.73 mm·y^{-1}, about half of which is attributed to a decrease in Surface Mass Balance (SMB) (4) that is expected to continue throughout this century and beyond (5). Over this period, ice dynamic changes contributed about equally to total mass loss, but extrapolating this trend over the next century or two is much more uncertain because of the incomplete understanding of the physical forcing mechanisms responsible for observed flow acceleration and thinning of marine-terminating outlet glaciers. For example, the speedup of Jakobshavn Isbræ, which started in the late 1990s, has been attributed to the disintegration of the floating tongue and loss of buttressing (6), triggered by increased basal melt due to the intrusion of warm water into the fjord (7), or to the weakening of the ice in the lateral shear margins and perhaps a change in the properties at the bed (8).

Acknowledging that such predictions are at a "fairly early stage," the Fifth Assessment Report, issued by the Intergovernmental Panel on Climate Change, includes a projected total SLR by 2100 of 14–85 mm, attributed to dynamic changes of the GrIS for the different future warming scenarios (5). This estimate is based on modeled evolution of four key outlet glaciers (Jakobshavn, Helheim, Kangerlussuaq, and Petermann), whose projected response is scaled up to all Greenland outlet glaciers (9–11). There are two concerns with this approach. First, understanding the dynamic response of marine-terminating outlet glaciers to a warming climate—a prerequisite for deriving reliable mass balance projections—remains a major challenge (12–14). Second, considering the complexity of recent behavior of outlet glaciers (15, 16), it is far from clear how four well-studied glaciers represent all of Greenland's outlet glaciers and whether their response can be scaled up to the entire ice sheet. For example, in southeast Greenland, a region that accounted for more than half of the total 2005 GrIS mass loss (17), many outlet glaciers rapidly adjusted to a new equilibrium by 2006 (16, 18). At the same time, dynamic mass loss continued, or even accelerated, from Jakobshavn Isbræ, the northwest Greenland outlet glaciers and the North East Greenland Ice Stream (19–21).

For improving ice sheet models and sea-level predictions, it is imperative to quantitatively investigate dynamic ice loss processes. Recent results from the Gravity Recovery and Climate Experiment (GRACE) satellite gravimetry (22, 23) and input–output method (IOM, SMB minus discharge) (24) revealed a spatially shifting pattern of annual mass loss during 2003–2010, attributed to a regionally variable interplay of ocean and surface processes as well as ice dynamics. However, the limited spatial resolution of these techniques does not permit documenting the spatial pattern of changes on individual glaciers. Precise elevation measurements, combined with SMB estimates, offer a possibility to increase the spatial resolution of the ice sheet

Significance

We present the first detailed reconstruction of surface elevation changes of the Greenland Ice Sheet from NASA's laser altimetry data. Time series at nearly 100,000 locations allow the characterization of ice sheet changes at scales ranging from individual outlet glaciers to larger drainage basins and the entire ice sheet. Our record shows that continuing dynamic thinning provides a substantial contribution to Greenland mass loss. The large spatial and temporal variations of dynamic mass loss and widespread intermittent thinning indicate the complexity of ice sheet response to climate forcing, strongly enforcing the need for continued monitoring at high spatial resolution and for improving numerical ice sheet models.

Author contributions: B.M.C. designed research; B.M.C., A.F.S., G.B., K.D., S.R., and S.N. performed research; A.F.S., M.R.v.d.B., S.B.S., and J.H.v.A. contributed new data/analytic tools; B.M.C., C.J.v.d.V., G.B., and S.R. analyzed data; and B.M.C., A.F.S., and C.J.v.d.V. wrote the paper.

The authors declare no conflict of interest.

*This Direct Submission article had a prearranged editor.

Freely available online through the PNAS open access option.

[1]To whom correspondence should be addressed. Email: bcsatho@buffalo.edu.

This article contains supporting information online at www.pnas.org/lookup/suppl/doi:10.1073/pnas.1411680112/-/DCSupplemental.

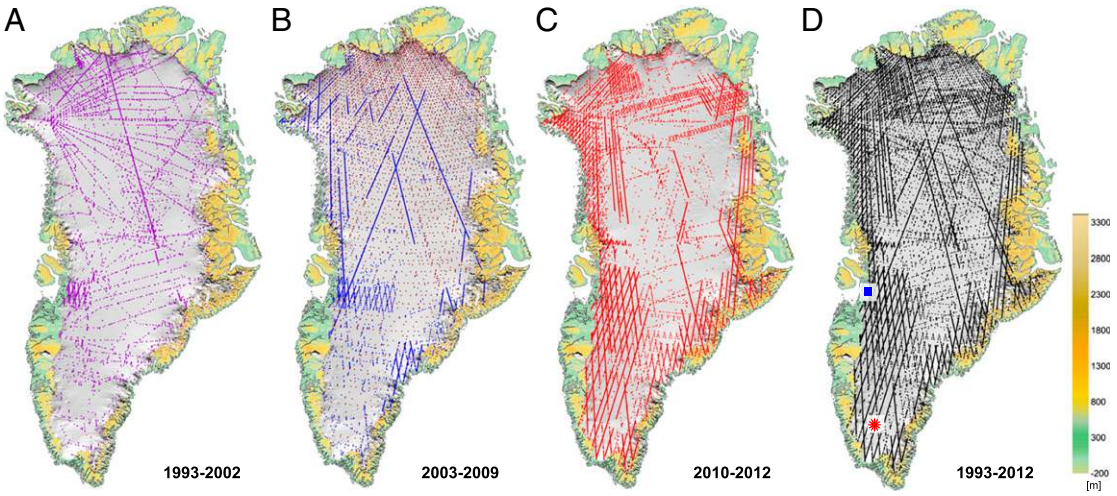

Fig. 1. Location of GrIS elevation time series according to the main data sets used for SERAC reconstruction. (*A*) PARCA ATM (1993–2003) and ICESat (purple); (*B*) PARCA ATM (2003–2009) and ICESat (blue), ICESat crossovers only (brown); (*C*) OIB ATM/LVIS (2009–2012) and ICESat (red); and (*D*) combined: all solutions (black). GrIS is shown in gray, and land surface with local ice caps and glaciers is in green/brown hues. Symbols in *D* mark the locations of elevation change time series shown in Fig. S1.

elevation change and ice dynamics records. Repeat altimetry and stereo imaging have long been used to monitor the cryosphere, mostly for mapping multiyear average elevation changes (2, 25, 26), but neglecting the reconstruction of detailed temporal histories. As surface elevation observations are often collected with varying spatial resolutions and at slightly different locations, the derivation of accurate elevation histories has remained a challenging task.

Here we present, to our knowledge, the first detailed reconstruction of GrIS elevation changes, derived from NASA's 1993–2012 laser altimetry record. Available at nearly 100,000 locations and partitioned into thickness changes associated with SMB variations and dynamic processes, our elevation change history characterizes ice sheet processes on spatial scales ranging from individual outlet glaciers to larger drainage basins and the entire ice sheet. By retaining the original temporal resolution, it is suitable for investigating rapid ice dynamic responses to contemporary atmospheric and oceanic forcings, processes that are still poorly understood (13, 14). Our reconstruction reveals the complexity of ice sheet response to climate forcing. We detect similar, simultaneous elevation changes over distances up to 500 km, indicating climate control on recent mass changes. However, we also show that outlet glacier dynamics exhibits large spatiotemporal variability, suggesting that the response of individual outlet glaciers likely depends on local conditions, such as bed topography and local climate conditions.

Results

Reconstruction of GrIS Elevation Change. As part of NASA's Program for Arctic Regional Climate Assessment (PARCA), airborne laser altimetry surveys began in 1993 with NASA's Airborne Topographic Mapper (ATM) (27). However, investigations of ice sheet mass balance and related sea level rise were hampered by the lack of spatially comprehensive elevation time series. To remedy this, NASA launched the Ice, Cloud and land Elevation Satellite (ICESat) mission in 2003 with the primary goal of measuring elevation changes over the polar ice sheets with sufficient accuracy to assess their impact on global sea level (28). After a successful period of obtaining accurate elevations of the Greenland and Antarctic ice sheets, ICESat's last campaign ended on October 11, 2009. The successor, ICESat-2, is expected to be launched in 2017. To "bridge" the intervening time without satellite laser altimetry data, NASA started Operation IceBridge mission (OIB), which has been gathering laser altimetry data using the ATM and the Land, Vegetation and Ice Sensor [LVIS (29)] airborne systems in both polar regions.

We developed the novel Surface Elevation Reconstruction and Change detection (SERAC) method to determine surface elevation changes at ICESat crossover areas (intersections of ascending and descending ICESat tracks) (30). The method is based on fitting an analytical function to the laser points of a surface patch, such as a crossover area, of ~1 km^2 in size. The surface patches of different time epochs at the same crossover area are related to each other; we have introduced the constraint that within a surface patch, the shape of the ice sheet remains the same over the entire observation period; only its absolute elevation changes. The least-squares adjustment of SERAC simultaneously determines one set of best-fit shape parameters and a time series of elevations for all time epochs involved, together with rigorous error estimates (ref. 30, *SI Text*, and Fig. S1).

Originally limited to ICESat crossover areas only, SERAC has been extended to provide solutions along the ICESat ground tracks by combining ICESat data with airborne laser altimetry data (31). In this way, the spatial density of surface elevation time series increases dramatically, as Fig. 1 vividly demonstrates. Fig. 1*B* depicts ICESat crossover locations (brown) and additional locations where 2003–2009 ATM and LVIS flights intersected or repeated ICESat ground tracks (blue). However, large gaps remain, especially in southern Greenland. Adding ATM data from the period 1993–2002 as well as ATM and LVIS data from 2010 to 2012 remedies this situation, resulting in a dense data set.

The fusion framework of SERAC offers other advantages. For example, inclusion of ATM and/or LVIS data that were collected during ICESat mission (2003–2009) increases the temporal resolution of the elevation change record. If data are available from earlier time periods, the time series are extended backward in time, before 2003. Using data from the OIB mission extends the time series toward the present.

Ultimately, by combining all NASA laser altimetry measurements, elevation time series are reconstructed at ~100,000 locations, resulting in a very dense coverage along ICESat ground tracks, especially in the ice sheet marginal region. Despite occasional cloud cover, ice sheet elevations were measured at least once during each of the 19 ICESat operational periods at most crossover locations (30). Thus, by adding ATM and LVIS

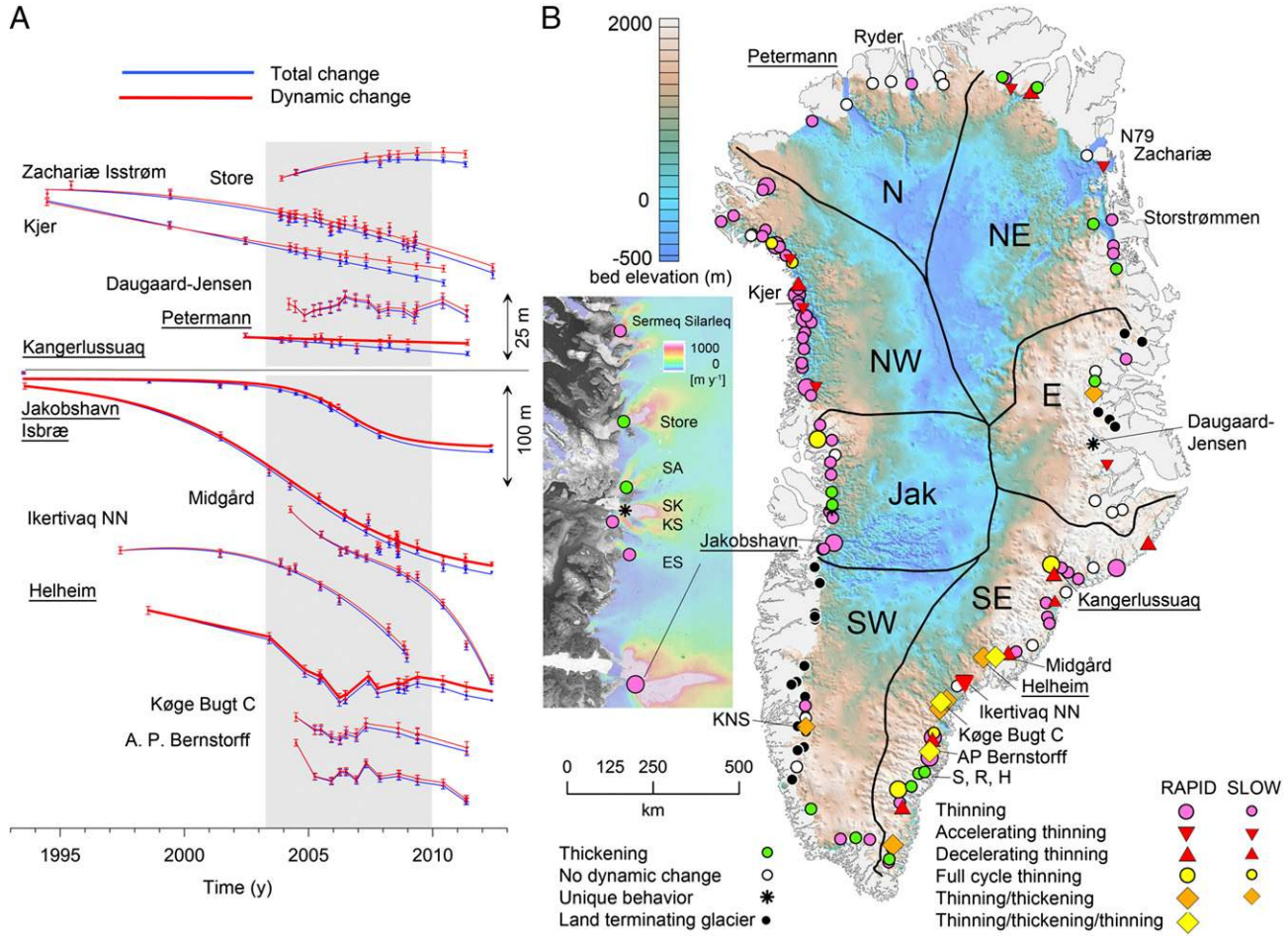

Fig. 2. Classification of outlet glaciers based on dynamic thickness change pattern. (*A*) Thickness change time series derived from the combined ICESat/ATM/LVIS altimetry record (1993–2012) illustrating different dynamic outlet glacier behaviors. Thickening: Store Glacier (6); no dynamic change: Petermann Glacier (78); decelerating thinning: Kjer Glacier (83); accelerating thinning: Zachariæ Isstrom (51) and Ikertivaq NN (46); full cycle thinning: Jakobshavn Isbræ (1); thinning with varying rate: Midgård Glacier (121); thinning, thickening, and thinning with abrupt termination of initial thinning: Helheim (3), Koge Bugt C (4), and A. P. Bernstorff (12) glaciers; unique pattern with periodic thinning and thickening: Daugaard-Jensen Glacier (8). Numbers in parentheses are ID numbers from ref. 32 and in Table S1. Gray box marks the duration of the ICESat mission, and glacier locations are shown in *B*. Dynamic thickness changes of the four large outlet glaciers, Jakobshavn Isbræ, Kangerlussuaq, Helheim, and Petermann glaciers, underlined in the figure, are modeled in refs. 9–11. (*B*) Distribution of different outlet glacier behavior types over a background of ice sheet bed elevation from ref. 45. *Inset* shows the detailed pattern north of Jakobshavn Isbræ overlain on ice velocities from ref. 32. Abbreviations mark the following outlet glaciers: Sermeq Avannarleq (SA, 53), Sermeq Kujalleq (SK, 13), Kangilerngata Sermia (KS, 52), Eqip Sermia (ES, 90), Kangiata Nunaata Sermia (KNS, 36), Skinfaxe (S, 82), Rimfaxe (R, 58), and Heimdal (H, 39) glaciers. See Table S1 for a complete list of glaciers and their classification based on 2003–2009 and 1993–2012 dynamic thickness change patterns.

measurements, a dense temporal sampling is obtained for 2003–2009, with additional points from LVIS and ATM extending most of the curves beyond ICESat's lifetime (Fig. 2*A* and Fig. S1). After removing the effect of vertical crustal motion due to Glacial Isostatic Adjustment (GIA; *SI Text*), we partition the ice thickness change time series into components associated with ice dynamics and SMB changes (*Materials and Methods*, *SI Text*, and Fig. S1).

The high spatial density of the new 1993–2012 elevation change record and the 91-d repeat cycle of ICESat allow for the investigation of the spatiotemporal pattern of ice sheet thickness change at different scales. The ice thickness change time series (Fig. 2*A* and Fig. S1) provides the highest resolution, suitable for characterizing the dynamic processes affecting individual outlet glaciers. The most recent compilation of GrIS ice velocities includes 242 outlet glaciers with a width greater than 1.5 km (32). We identified 130 of these glaciers with a 5- to 19-y-long altimetry record, out of which 115 are marine terminating (Tables S1 and S2). Average elevation change rates are found to be in good agreement with previous studies (*SI Text* and Table S3). However, we have shown that changes are typically nonlinear in time and most of the rapid changes occur during the ICESat mission (Fig. 2*A*). For many marine-terminating outlet glaciers, dynamic thickness change patterns are consistent with an inland propagation of dynamic thinning or thickening initiated at the coast (Fig. S2 *A* and *B*). Some glaciers exhibit a more complicated behavior, however. For example, Størstrommen, L. Bistrup Bræ, and Marie Sophie glaciers, which are quiescent surging glaciers, have a characteristic pattern with large, steady thickening at their source regions, as ice accumulates upstream of the reduced flow, and thinning below the area where the surge was initiated (Fig. S2*C* and Table S1), while the complex elevation change pattern of Hagen Bræ might indicate an ongoing surge (Table S1). Short-term, sometimes cyclic elevation changes occurred on 15 outlet glaciers, all marine terminating (*SI Text* and Table S1), and may indicate control from subglacial hydrology or are perhaps related to the drainage of proglacial lakes (e.g., Daugaard-Jensen Glacier, Fig. S2*D*). Dynamic thinning was negligible on 13 out of the 15 land-terminating glaciers (*SI Text* and Tables S1 and S2).

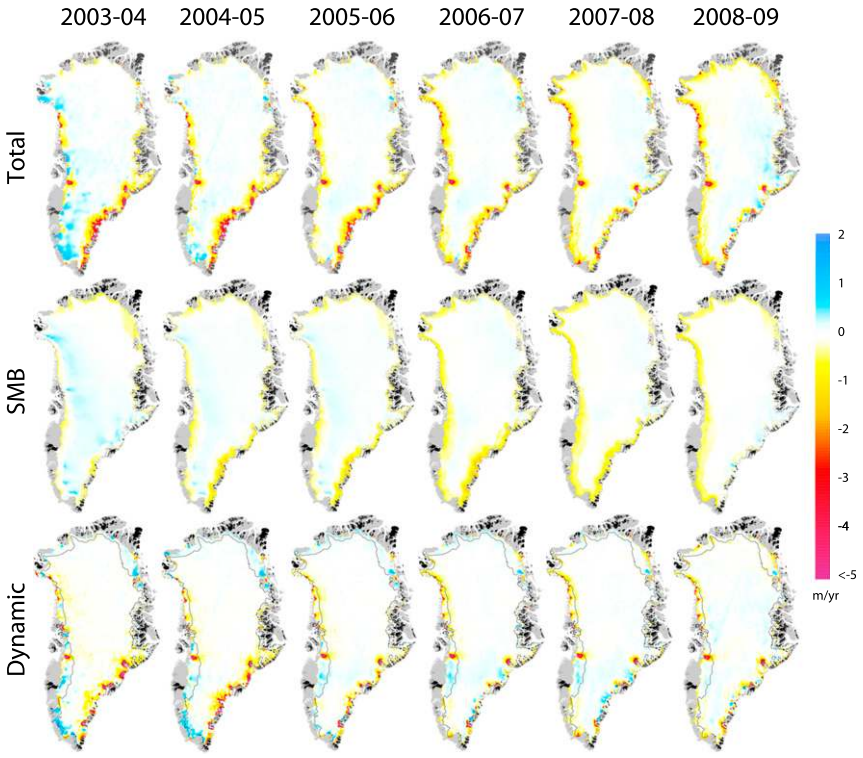

Fig. 3. Annual total, SMB-related, and ice dynamics-related thickness change rates of the GrIS for 2003–2009 balance years from ICESat, ATM and LVIS laser altimetry observations (see Fig. 1 for locations of elevation change records). Dotted lines on the dynamic thickness change maps mark the ELA (average 2003–2009 SMB = 0). Ice sheet boundary is from ref. 46, and black regions show weakly or not connected glaciers and ice caps. Balance years start on September 1 and end on August 31 of the following year. See Movie S1 for a higher-resolution, animated version of the figure.

To facilitate interpretation, glaciers are divided into the following distinct groups according to their dynamic thickness change pattern in 2003–2009: thinning with steady or slowly changing rates (accelerating, decelerating, full cycle thinning); slow or rapid thinning that abruptly terminated and was followed by thickening and in some cases by resumed thinning; thickening; unique elevation change pattern; and no dynamic change (Fig. 2 and Table S1).

To investigate drainage basin-scale processes, we compute annual ice thickness change rates at each surface patch location from a polynomial fit through the thickness changes reconstructed by SERAC (30) and partition these rates into changes associated with SMB and ice dynamics (*Materials and Methods*, *SI Text*, and Fig. S1). The interpolated annual thickness change rate grids show intricate and rapidly changing patterns (Fig. 3 and Movie S1). To quantify these, volume and mass change rates of the main ice sheet regions are calculated (Fig. 4 and Tables S4 and S5).

GrIS Ice Thickness Change and Mass Loss Patterns, 1993–2012. We estimated a mean annual GrIS loss of 243 ± 18 $Gt{\cdot}y^{-1}$ (277 ± 7 $km^3{\cdot}y^{-1}$), equivalent to 0.68 ± 0.05 $mm{\cdot}y^{-1}$ SLR for 2003–2009 (Tables S4 and S5). This mass loss and its interannual variability are in good agreement with the reconciled GrIS mass loss estimate derived from a combined ensemble of laser altimetry, GRACE, and IOM data (3). However, we detected higher average mass loss and interannual variability than the laser altimetry results included in ref. 3, bringing the laser altimetry, GRACE, and IOM estimates closer to each other (ref. 3, *SI Text*, and Tables S5 and S6), thus reconciling the previously perceived inconsistencies among different methods. Dynamic thinning contributed 48% to the total mass loss, which is the same as reported in ref. 4. Dynamic loss was largest in 2004–2005, followed by a gradual decrease that was balanced by accelerating SMB loss (Fig. 4). However, at the same time, the relative contributions of major drainage basins changed significantly (Figs. 3 and 4), indicating that processes acting on time scales of less than a decade have a significant effect on ice sheet mass loss and related SLR. The only region exhibiting steady mass loss from 2003 to 2009 was Jakobshavn, while mass loss decelerated from southeast and east Greenland and accelerated from the rest of Greenland, confirming the pattern reconstructed from GRACE observations (23). In this section, we review the dynamic behavior of individual marine-terminating outlet glaciers and explore their impact on drainage basin scale dynamic mass changes.

Almost half of the total 2003–2009 GrIS mass loss originated from southeast Greenland (Table S5). Glaciers in this sector thinned rapidly between 2003 and 2005, reaching their peak discharge in 2005 (refs. 16 and 18, Figs. 3 and 4). During this time, dynamic thinning extended far inland, up to the ice divide in some areas (Movie S1), maintaining a pattern that started in the 1970s or earlier (33). This large dynamic loss, peaking at 166 ± 31 $Gt{\cdot}y^{-1}$, was a major source of the record negative GrIS mass balance of 293 ± 38 $Gt{\cdot}y^{-1}$ in 2004–2005. As flow acceleration slowed down or reversed to deceleration after 2005 (16), thinning rates decreased, and several glaciers, for example Helheim Glacier, started to thicken (Fig. 2). At the same time, the long-term trend of high-elevation thinning also reversed, and by 2007–2008, most of southeast GrIS exhibited dynamic thickening (Fig. 3 and Movie S1). By 2007–2008, the ice loss rate from the southeast GrIS dropped to less than one third of its peak value, as a result of a diminishing dynamic mass loss. However, the slowdown and thickening of outlet glaciers was short lived, as they resumed acceleration (16) and thinning by 2009 (Fig. 2). In addition to widespread short-term changes, outlet glacier thinning shows a large spatial variability in southeast Greenland, much like the velocity record (16), indicating an intricate interplay of regional and local forcings and controls. For example, rapid thickening of outlet glaciers within a region extending to 500 km in north–south direction, and including Helheim, Køge Bugt C, and A. P. Bernstorff glaciers, started at the same time and exhibited very similar patterns (Fig. 2), suggesting regional climate controls. Meanwhile, other glaciers in the region, such as Midgård and Ikertivaq glaciers, continued to thin, losing

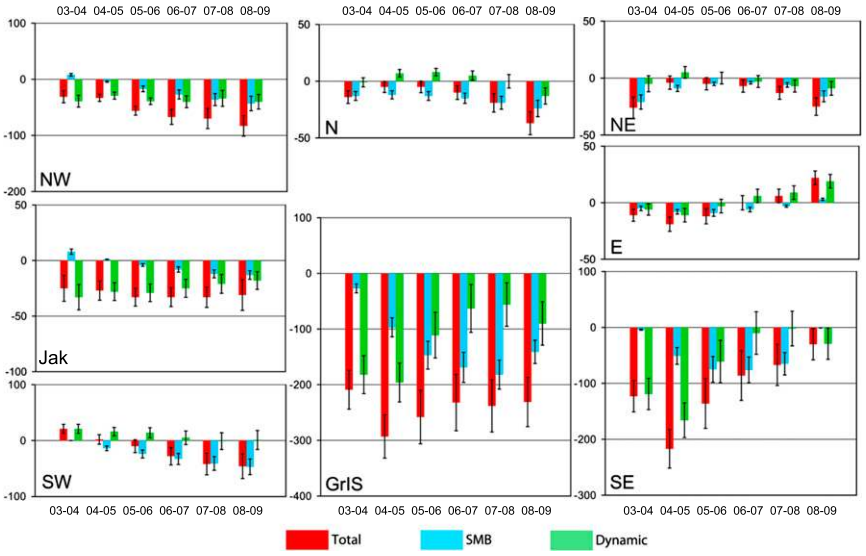

Fig. 4. Annual mass change rates in gigatons per year for major drainage basins shown in Fig. 2*B*. Annual total mass change rates from laser altimetry (red) are partitioned into mass changes due to SMB (blue) and ice dynamics (green). Annual mass change rates and their error estimates are listed in Table S5.

ice at increasing rates. In contrast, Heimdal, Rimfaxe, and Skinfaxe glaciers, maintaining steady calving front positions since 1933 (34), have been thickening (Fig. 2*B*).

Concurrent with the 2003–2005 rapid thinning of the southeast region, the adjacent southwest basin was thickening (Fig. 3 and Movie S1). This positive mass balance was due to the dynamic thickening of the land-terminating ice sheet margin, interpreted as a reaction to increasing accumulation during an ice sheet readvance 4,000 y ago (35). Increasing dynamic thinning of major outlet glaciers (e.g., Kangiata Nunata Sermia, Fig. 2*B*) and accelerating SMB loss resulted in an overall negative mass balance of this region by 2005 (Fig. 4).

Annual mass loss of the Jakobshavn region was steady at a rate of 30 ± 4 Gt·y^{-1}, dominated by losses caused by the continuing speedup and corresponding thinning of Jakobshavn Isbræ (19). Thinning rates started to decrease near its calving front in 2007 (Fig. 2*A* and Fig. S2*A*), indicating an adjustment to new environmental conditions and signaling a potential future mass loss decrease. The outlet glaciers draining to the narrow fjords north of Jakobshavn Isbræ show a complex spatial pattern of dynamic elevation changes in 2003–2009 (Fig. 2*B*, *Inset*).

In northwest Greenland, ice loss has accelerated linearly from 31 ± 11 Gt·y^{-1} to 83 ± 18 Gt·y^{-1} between 2003 and 2009, due to increasingly negative SMB anomalies and a steady dynamic loss (Fig. 4 and Table S5). Our long-term altimetry record shows that dynamic thinning has been steady or accelerated on most outlet glaciers during the last 15–20 y (e.g., Kjer Glacier, Fig. 2). This is consistent with the steady increase of ice discharge between 2000 and 2010 detected by refs. 16 and 36 and contradicts a previous reconstruction that indicated a stable period between 1992 and 2005, followed by dynamic thinning and increased discharge (37).

The three other major regions (north, east, and northeast) remained dynamically relatively inactive over the period of 2003–2009. Ice sheet mass balance had a similar trend in north and northeast, where a decreasing negative balance was followed by a slow mass loss increase since 2005 due to a combination of increasing negative SMB and increasing dynamic loss. Thinning rates of north and northeast Greenland outlet glaciers are relatively small (<5 m·y^{-1}). However, thinning of Ryder Glacier and Zachariæ Isstrom (Fig. 2) at current or increasing rates could unground their large ice plains within a few decades as continuing thinning brings the ice closer to flotation (21, 26). The resulting speedup over large areas would ultimately cause a significant mass loss from the deep central part of the GrIS. Elevation changes were also small, but increasingly positive, in east Greenland, resulting in a positive mass balance by 2007.

Discussion

The spatiotemporal pattern of annual ice sheet thickness change rates shows clear trends as well as interannual variations (Fig. 3). Averaged over the entire GrIS, the central, high-elevation part was slightly thickening during the entire time, with interannual variations corresponding to SMB anomalies. Dynamic thinning was most pronounced below the equilibrium line altitude (ELA), with the largest thinning rates observed on Jakobshavn, Helheim, and Kangerlussuaq glaciers and in southeast and northwest Greenland. The dynamic behavior of dominant outlet glaciers determines the mass loss pattern of major drainage basins (Figs. 2 and 4). Dynamic mass loss and gain varied rapidly in southeast Greenland where most glaciers, fed by short and narrow drainage basins and reaching the fjords through narrow and deep bedrock channels, appear to adjust in 3–4 y to changing boundary conditions. In contrast, most outlet glaciers in northwest Greenland have been exhibiting uninterrupted long-term dynamic thinning, in some cases for more than 15 y (e.g., Kjer Glacier, Fig. 2). Here, outlet glaciers drain a 50- to 80-km-wide coastal region with deep channels incised into a relatively flat topography only slightly above sea level, facilitating a rapid propagation of outlet glacier thinning to the surrounding slower flowing regions.

Dynamic thinning of outlet glaciers exhibits a large spatial and temporal variability (Fig. 2, *SI Text*, and Tables S1 and S2). Different glacier groups are not confined to specific regions, and some nearby outlet glaciers show very different temporal behavior. This casts doubt on models that attribute observed flow accelerations and thinning to a single mechanism. Rather, these observations suggest that response of individual glaciers to external forcings is more involved and may depend on local geometry factors such as bed topography and size of the drainage basin. The rapid reversal of thinning to thickening in southeast Greenland over a region that extends far inland suggests that mass changes might occur in response to processes acting over larger areas, rather than near the grounding line only. This behavior has not been captured in existing ice flow models and may be linked to rapid changes in subglacial hydrology affecting the sliding speed (38, 39). The majority of GrIS mass loss during the period of 2003–2009 is due to thinning of southeast and northwest Greenland glaciers with small to moderately sized drainage basins, rather than the four large modeled glaciers (Fig. S3*A*). Moreover, mass loss is not proportional with drainage basin

area (Fig. S3*B*), as was assumed by ref. 10. These findings challenge the practice of estimating the future dynamic contribution of the entire GrIS to global sea level based on modeled behavior of three or four major outlet glaciers, one of which (Petermann Glacier) did not show much dynamic change over the period considered.

Our record shows that continuing dynamic thinning provides a substantial contribution to Greenland mass loss. The large spatial and temporal variations of dynamic mass loss and widespread intermittent thinning indicate the complexity of ice sheet response to climate forcing, pointing to the need for continued monitoring of the GrIS at high spatial resolution.

Materials and Methods

Elevation change time series are reconstructed from ICESat, ATM, and LVIS laser altimetry data by SERAC (see *SI Text* for details on the data sets and their accuracies). They are corrected for GIA and partitioned into components corresponding to SMB anomalies, changes in firn compaction rates, and ice dynamics (Fig. S1). GIA-related vertical crustal motion estimates are from ref. 40. Regional Atmospheric Climate Model (RACMO2/GR) SMB anomalies (41) are converted into ice thickness change using surface firn densities derived by a simple empirical model (42). This model accounts for the formation of ice lenses in the snowpack assuming that all retained meltwater refreezes at the same annual layer. Variations of firn compaction rates are from a 5-km by 5-km gridded model (43) forced by the output from the HIRHAM5 Regional Climate Model (44). Annual rates of total, SMB-related, and dynamic ice thickness change rates are estimated from polynomial approximations of the time series, and are gridded into 2-km-resolution grids using ordinary kriging with an exponential, isotropic variogram model. To obtain mass changes, we converted dynamic thickness changes to mass changes with an assumed ice density of 917 $kg \cdot m^{-3}$. Total mass changes were then estimated as the sum of dynamic and SMB mass changes. Details on the computation of the total, SMB, and dynamic thickness change time series, as well as thickness, volume, and mass change rates, together with their error estimates, are presented in *SI Text*. Comparison with published thickness change rates (Table S3) and mass balance rate estimates (Table S6) confirms the accuracy of our results.

ACKNOWLEDGMENTS. ICESat, ATM, and LVIS data were collected by NASA's PARCA, ICESat, and OIB missions and distributed by the National Snow and Ice Data Center. B.M.C., A.F.S., C.J.v.d.V., K.D., G.B., S.R., and S.N. acknowledge support by NASA's Polar Program under Grants NNX10AV13G, NNX11AR23G, and NNX12AH15G. M.R.v.d.B. and J.H.v.A. acknowledge support from the Netherlands Polar Program of Netherlands Organization for Scientific Research Division for the Earth and Life Sciences (NWO-ALW) and EU FP7 program ice2sea.

1. Rignot E, Velicogna I, van den Broeke MR, Monaghan A, Lenaerts J (2011) Acceleration of the contribution of the Greenland and Antarctic ice sheets to sea level rise. *Geophys Res Lett* 38(5):L05503.
2. Zwally HJ, et al. (2011) Greenland ice sheet mass balance: Distribution of increased mass loss with climate warming; 2003-07 versus 1992-2002. *J Glaciol* 57(201):88–102.
3. Shepherd A, et al. (2012) A reconciled estimate of ice-sheet mass balance. *Science* 338(6111):1183–1189.
4. van den Broeke M, et al. (2009) Partitioning recent Greenland mass loss. *Science* 326(5955):984–986.
5. Church JA, et al. (2013) Sea level change. *Climate Change 2013: The Physical Science Basis. Contribution of Working Group I to the Fifth Assessment Report of the Intergovernmental Panel on Climate Change*, eds Stocker TF, et al. (Cambridge Univ Press, New York), pp 1137–1216.
6. Joughin I, et al. (2008) Continued evolution of Jakobshavn Isbrae following its rapid speedup. *J Geophys Res* 113(F4):F04006.
7. Holland DM, Thomas RH, De Young B, Ribergaard MH, Lyberth B (2008) Acceleration of Jakobshavn Isbrtriggered by warm subsurface ocean waters. *Nat Geosci* 1(10):659–664.
8. van der Veen CJ, Plummer JC, Stearns LA (2011) Controls on the recent speed-up of Jakobshavn Isbræ, West Greenland. *J Glaciol* 57(204):770–782.
9. Price SF, Payne AJ, Howat IM, Smith BE (2011) Committed sea-level rise for the next century from Greenland ice sheet dynamics during the past decade. *Proc Natl Acad Sci USA* 108(22):8978–8983.
10. Nick FM, et al. (2013) Future sea-level rise from Greenland's main outlet glaciers in a warming climate. *Nature* 497(7448):235–238.
11. Goelzer H, et al. (2013) Sensitivity of Greenland ice sheet projections to model formulations. *J Glaciol* 59(216):733–749.
12. Joughin I, Alley RB, Holland DM (2012) Ice-sheet response to oceanic forcing. *Science* 338(6111):1172–1176.
13. Straneo F, et al. (2013) Challenges to understanding the dynamic response of Greenland's marine terminating glaciers to oceanic and atmospheric forcing. *Bull Am Meteorol Soc* 94(8):1131–1144.
14. Straneo F, Heimbach P (2013) North Atlantic warming and the retreat of Greenland's outlet glaciers. *Nature* 504(7478):36–43.
15. McFadden EM, Howat IM, Joughin I, Smith BE, Ahn Y (2011) Changes in the dynamics of marine terminating outlet glaciers in west Greenland (2000–2009). *J Geophys Res* 116(F2):F02022.
16. Moon T, Joughin I, Smith B, Howat I (2012) 21st-century evolution of Greenland outlet glacier velocities. *Science* 336(6081):576–578.
17. Rignot E, Kanagaratnam P (2006) Changes in the velocity structure of the Greenland Ice Sheet. *Science* 311(5763):986–990.
18. Howat IM, Joughin I, Scambos TA (2007) Rapid changes in ice discharge from Greenland outlet glaciers. *Science* 315(5818):1559–1561.
19. Howat IM, et al. (2011) Mass balance of Greenland's three largest outlet glaciers, 2000–2010. *Geophys Res Lett* 38(12):L12501.
20. Khan SA, Wahr J, Bevis M, Velicogna I, Kendrick E (2010) Spread of ice mass loss into northwest Greenland observed by GRACE and GPS. *Geophys Res Lett* 37(6):L06501.
21. Khan SA, et al. (2014) Sustained mass loss of the northeast Greenland ice sheet triggered by regional warming. *Nat Clim Change* 4(4):292–299.
22. Harig C, Simons FJ (2012) Mapping Greenland's mass loss in space and time. *Proc Natl Acad Sci USA* 109(49):19934–19937.
23. Luthcke SB, et al. (2013) Antarctica, Greenland and Gulf of Alaska land-ice evolution from an iterated GRACE global mascon solution. *J Glaciol* 59(216):613–631.
24. Sasgen I, et al. (2012) Timing and origin of recent regional ice-mass loss in Greenland. *Earth Planet Sci Lett* 333:293–303.
25. Pritchard HD, Arthern RJ, Vaughan DG, Edwards LA (2009) Extensive dynamic thinning on the margins of the Greenland and Antarctic ice sheets. *Nature* 461(7266):971–975.
26. Thomas R, Frederick E, Krabill W, Manizade S, Martin C (2009) Recent changes on Greenland outlet glaciers. *J Glaciol* 55(189):147–162.
27. Krabill WB, et al. (2002) Aircraft laser altimetry measurement of elevation changes of the Greenland ice sheet: Technique and accuracy assessment. *J Geodyn* 34(3):357–376.
28. Zwally HJ, et al. (2002) ICESat's laser measurements of polar ice, atmosphere, ocean, and land. *J Geodyn* 34(3):405–445.
29. Hofton MA, Blair JB, Luthcke SB, Rabine DL (2008) Assessing the performance of 20–25 m footprint waveform lidar data collected in ICESat data corridors in Greenland. *Geophys Res Let* 35(24):L24501.
30. Schenk T, Csathó B (2012) A new methodology for detecting ice sheet surface elevation changes from laser altimetry data. *IEEE Trans Geosci Remote Sens* 50(9):3302–3316.
31. Schenk T, Csatho B, van der Veen C, McCormick D (2014) Fusion of multi-sensor surface elevation data for improved characterization of rapidly changing outlet glaciers in Greenland. *Remote Sens Environ* 149:239–251.
32. Rignot E, Mouginot J (2012) Ice flow in Greenland for the International Polar Year 2008–2009. *Geophys Res Lett* 39(11):L11501.
33. Thomas R, et al. (2001) Mass balance of higher-elevation parts of the Greenland ice sheet. *J Geophys Res* 106(D24):33707–33716.
34. Bjørk AA, et al. (2012) An aerial view of 80 years of climate-related glacier 278 fluctuations in southeast Greenland. *Nat Geosci* 5(6):427–432.
35. Huybrechts P (1994) The present evolution of the Greenland ice sheet: An assessment by modelling. *Global Planet Change* 9(1):39–51.
36. Enderlin EM, et al. (2014) An improved mass budget for the Greenland ice sheet. *Geophys Res Lett* 41(3):866–872.
37. Kjær KH, et al. (2012) Aerial photographs reveal late-20th-century dynamic ice loss in northwestern Greenland. *Science* 337(6094):569–573.
38. Schoof C (2010) Ice-sheet acceleration driven by melt supply variability. *Nature* 468(7325):803–806.
39. Koenig LS, Mige C, Forster RR, Brucker L (2014) Initial in situ measurements of perennial meltwater storage in the Greenland firn aquifer. *Geophys Res Lett* 41(1):81–85.
40. G A, Wahr J, Zhong S (2013) Computations of the viscoelastic response of a 3-D compressible Earth to surface loading: An application to Glacial Isostatic Adjustment in Antarctica and Canada. *Geophys J Int* 192(2):557–572.
41. van Angelen JH, van den Broeke MR, Wouters B, Lenaerts JTM (2014) Contemporary (1960–2012) evolution of the climate and surface mass balance of the Greenland ice sheet. *Surv Geophys* 35(5):1155–1174.
42. Reeh N, Fisher DA, Koerner RM, Clausen HB (2005) An empirical firn-densification model comprising ice lenses. *Ann Glaciol* 42(1):101–106.
43. Sørensen LS, et al. (2011) Mass balance of the Greenland ice sheet (2003–2008) from ICESat data – the impact of interpolation, sampling and firn density. *Cryosphere* 5(1):173–186.
44. Lucas-Picher P, et al. (2012) Very high resolution regional climate model simulations over Greenland: Identifying added value. *J Geophys Res* 117(D2):D02108.
45. Bamber JL, et al. (2013) A new bed elevation dataset for Greenland. *Cryosphere* 7(2):499–510.
46. Rastner P, Bolch T, Molg N, Machguth H, Paul F (2012) The first complete glacier inventory for the whole of Greenland. *Cryosphere* 6(4):1483–1495.

Supporting Information

Csatho et al. 10.1073/pnas.1411680112

SI Text

Computation of Surface Elevation, Volume, and Mass Changes and Partitioning Them into SMB-, Firn Compaction-, and Ice Dynamics-Related Components

Assuming steady-state flow during the period of 1960–1990 and negligible basal mass balance and internal melt rate changes, we obtain the following expression from equation 8.77 in ref. 1 for partitioning the measured surface elevation changes into components related to vertical crustal motion, SMB, firn compaction, and ice dynamics:

$$H_{s,total}(t_0) - \underbrace{t_0\, v_{br}}_{VerticalCrustalMotion} = h_{total}(t_0) = \underbrace{\sum_{i=1}^{I-1}\sum_{j=1}^{12}\frac{b_{anomaly,i,j}}{\rho_{s,i}} + \sum_{j=1}^{J}\frac{b_{anomaly,I,j}}{\rho_{s,I}}}_{SMB\ Thickness\ Change} + \underbrace{t_0\, v_{f,change}}_{FirnCompaction} + \underbrace{h_{dynamic}(t_0)}_{DynamicThicknessChange} \quad [S1]$$

where

t_0, time elapsed since the start of the record, in years;

I, number of full balance years before t_0—each balance year starts on September 1 and ends on August 31 of the next year;

J, number of months in the last balance year;

$H_{s,total}(t_0)$, total surface elevation change reconstructed by SERAC at time t_0, in meters;

v_{br}, vertical crustal velocity due to GIA and elastic rebound, in meters per year;

$h_{total}(t_0)$, total ice thickness change at time t_0, in meters;

$b_{anomaly,i,j}$, monthly SMB anomaly, in kilograms per square meter per month;

$\rho_{s,i}$, density of annual surface firn layer, in kilograms per cubic meter;

$v_{f,change}$, change in vertical ice velocity due to changes in firn-compaction velocity, in meters per year; and

$h_{dynamic}(t_0)$, dynamic ice thickness change at time t_0 due to changes in flux divergence, in meters per year.

Total ice thickness change ($h_{total}(t_0)$) is calculated from the total surface elevation change ($H_{s,total}(t_0)$) by removing the effect of vertical crustal motion.

To estimate the ice thickness change related to SMB, monthly SMB anomalies ($b_{anomaly,i,j}$) are computed from RACMO2/GR SMB anomalies (2, 3) assuming ice sheet equilibrium in 1960–1990. Surface firn densities are estimated by an empirical model that accounts for the formation of ice lenses in the snowpack (4, 5). This model assumes that all retained meltwater (Superimposed Ice Remaining at the end of the melt season (SIR) = melt − runoff) refreezes at the same annual layer in the end of each balance year (August 31), giving

$$\rho_{s,i} = \frac{\rho_0}{1 - \frac{SIR_i}{b_i}\left(1 - \frac{\rho_0}{\rho_{ice}}\right)} \quad [S2]$$

where

SIR_i, amount of refrozen ice, estimated as the difference between the annual melt and runoff;

b_i, annual net SMB;

ρ_{ice}, density of ice, selected as 917 kg m^{-3}; and

ρ_0, temperature-dependent density of new firn before the formation of ice lenses, in kilograms per cubic meter.

The density of the new firn is calculated from the following empirical relationship: $\rho_0 = 625 + 18.7T_f + 0.293T_f^2$ and $T_f = TMA + 26.6SIR$, where T_f is the firn temperature at 10 m depth and TMA is the mean annual temperature from ref. 2. Annual melt, runoff, and net SMB are calculated for balance years from monthly RACMO2/GR estimates (2, 3).

Ice dynamics-related thickness change [$h_{dynamic}(t_0)$] is calculated from Eq. **S1**, as the difference between the total ice thickness change and the sum of thickness changes related to SMB and firn compaction.

To obtain mass changes, first we convert the ice dynamics-related thickness change to ice dynamics-related mass change with an assumed ice density of 917 kg·m^{-3}. The total mass change is then estimated as the sum of this ice dynamics-related mass change and the SMB-related mass change from RACMO2/GR.

Annual rates of total, SMB-related, and ice dynamics-related thickness and mass changes are computed from polynomial approximations of the thickness and mass change time series.

Fig. S1 illustrates the computation of the discrete and polynomial representations of the elevation and thickness changes at two sites on the GrIS. Fig. S1*A* shows the total, SMB-related, and dynamic thickness changes as well as density estimates for a site located near the ice divide in south Greenland, where ice velocity is low and thickness changes are likely caused by SMB anomalies. The results in Fig. S1*B* refer to a site on Sermeq Avannarleq, an outlet glacier in west Greenland, located north of Jakobshavn Isbræ, where thinning is caused by the combined effect of ice dynamics and negative SMB anomalies.

Annual elevation and mass change rates derived at irregularly distributed SERAC surface patch locations (Fig. 1) are interpolated into 2-km-resolution grids (Fig. 3) using ordinary kriging with an exponential variogram model and masked by the ice sheet boundary from ref. 6. Annual volume and mass change estimates of major drainage basins, computed from these grids, are presented in Fig. 4, Fig. S3, and Tables S3 and S4.

Data

Ice Sheet Elevation Data.

ICESat satellite laser altimetry, 2003–2009. GLA05 Level-1B Global Waveform-based Range Corrections Data and GLA12 Level-2 Antarctic and Greenland Ice Sheet Altimetry Data, Release 633 data products were obtained from the National Snow and Ice Data Center (NSIDC) (7). We applied the Gaussian-Centroid, or G-C, offset correction, derived from GLA05, for the GLA12 product. This correction is to compensate a recently discovered mistake in computing the range from matching the centroid of the transmitted pulse with the peak position of the Gaussian fit to the returned pulse (8). Remaining systematic elevation errors,

also called ICESat intermission biases, can reach 20 cm for any single campaign, resulting in an erroneous trend (9). This trend ranges from 0.3 cm·y^{-1} to +2.2 cm·y^{-1}, but is expected to decrease by 0.92–1.90 cm·y^{-1} after applying the G-C offset correction (8). Due to the lack of a clear definition and magnitude of the intermission biases, we have not corrected for this error. Data from all operational periods, except L1A and L1B, are used. Parameters characterizing the ICESat waveform were examined to assess the precision of the elevation data. Poor-quality data, characterized by an apparent reflectivity of <0.1 or a waveform misfit of >0.035 V were excluded from the SERAC processing (10). We assume an accuracy of 0.05–0.2 m for single shots on land ice surfaces (11, 12).

ATM airborne laser altimetry, 1993–2012. ATM Level-2 Icessn Elevation, Slope, and Roughness products were obtained from NSIDC (13). Icessn is derived from the original dense measurements and contains elevations at the centers of three to five planar surface patches (platelets) covering the 150- to 250-m-wide swath scanned by ATM. An elaborate discussion about accuracy and precision of ATM observations can be found in refs. 14 and 15. The root-mean-square error (RMSE) value of the elevation accuracy of the platelet approximation is about 0.05–0.1 m (15).

LVIS airborne laser altimetry, 2007, 2009–2011. LVIS Level-2 Geolocated Surface Elevation products were obtained from NSIDC (16). We selected the parameter called elevation_high (elevation of the center of the highest mode in the waveform) to describe the ice sheet surface elevations. The reported horizontal accuracy is about 2 m (RMSE). The relative elevation precision and accuracy was determined by repeat LVIS flights. Footprints from two separate flights and closer than 1 m to each other were examined. The resulting SD of the test showed a SD of ±0.08 m. More information about accuracy and precision can be found in ref. 17.

Glacial Isostatic Adjustment. GIA-related vertical crustal motion estimates are from ref. 18, based on the ICE-5G global glacial reconstruction with a VM2 mantle viscosity model and given in a 1° by 1° grid. Estimates range from 2.7 to 4.6 mm·y^{-1} with errors that are negligible compared with elevation change errors.

Climate Data. Annual elevation changes due to changes in firn compaction velocity are from a 5- by 5-km gridded model (19), forced by the output from the HIRHAM5 Regional Climate Model (20). As it is difficult to quantify the error in the firn comparison model, we assume an error of 100% or at least 2 mm·y^{-1}. Note that this error is larger than that estimated by ref. 19, figure 4, to account for the modeling error.

Monthly SMB, melt, and runoff estimates for the period of 1960–2012 are from RACMO2/GR, given on an 11- by 11-km grid (2, 3). The accuracy of the RACMO2/GR SMB estimate is about 30% (2, 21). Mean annual surface temperature is provided on a 5- by 5-km grid (2).

Error Budget

Error of Ice Sheet Elevation and Ice Sheet Elevation Change ($\sigma_{H,s,total}$). The least-squares adjustment of SERAC produces unique values for the unknown parameters, such as the changing surface elevation and surface shape, and also indicates their precision (22). Assuming uncorrelated altimetry observations with random errors, we obtain the random errors of the estimated parameters from the variance–covariance matrix (inverse of the normal equation matrix) and the unbiased estimate of the unit variance, $\hat{\sigma}_o^2$ (23). The error of ice sheet elevation, $\sigma_{H,s,total}$, is related to the error of the elevation of a single laser altimetry observation, σ_L, through the equation $\sigma_{H,s,total} = \sigma_L/\sqrt{n}$, with n the number of observations. Typical values for $\sigma_{H,s,total}$ in regions higher up on the ice sheet are about 0.02 m. In lower-elevation regions, $\sigma_{H,s,total}$ reaches values up to 1.0 m or larger, partially due to a modeling error, as low-order polynomials, typically used to approximate the ice sheet surface within the surface patch (22), might not describe a crevassed area well.

Error of Annual Total Ice Thickness Change Rate ($\sigma_{\Delta h,total}$). Applying the general error propagation law for a polynomial fit through the elevations reconstructed from altimetry renders the errors associated with the fitted polynomial (ref. 22, equation 10). This error is different for every location where elevation time series are reconstructed by SERAC, and it depends mainly on the temporal distribution of the elevation measurements and their errors. We estimate an average ice thickness change rate error of 0.01 m·y^{-1} for the upper, dynamically inactive part of the ice sheet (velocity <50 m·y^{-1}, from ref. 24). Thickness change errors for the dynamic (velocity >50 m·y^{-1}), coastal regions within the major drainage basins of the ice sheet (Fig. 2) are assumed to be the following: an estimated error of 0.5 m·y^{-1} for north, northeast, and east drainage basins; 1 m·y^{-1} for northwest and southwest drainage basins; and 2 m·y^{-1} for Jak and southeast drainage basins.

Error of Annual Ice Dynamics-Related Thickness Change Rate ($\sigma_{\Delta h,dynamic}$). This error is estimated from the errors of the annual total and SMB-related ice thickness change rates in the following fashion:

$$\sigma_{\Delta h,dynamic} = \sqrt{\sigma^2_{\Delta h,total} + \sigma^2_{\Delta h,SMB} + \sigma^2_{\Delta h,firn}} \qquad \textbf{[S3]}$$

where $\sigma_{\Delta h,SMB}$ and $\sigma_{\Delta h,firn}$ are the errors of the annual SMB-related and firn compaction-related annual elevation change rate estimates, respectively.

To account for the errors of SMB anomalies, melt rate, runoff, and temperature estimates as well as for modeling errors in computing the surface firn density, we assume an error of 40% in the annual elevation change rates caused by SMB anomalies. Finally, we assume a firn compaction rate error of 100% or at least 2 mm·y^{-1} (see *Climate Data*).

Error of Annual Total Volume Change Rate of Large Drainage Basins ($\sigma_{\Delta V,Total,Basin}$). The error of the total volume change rate of major drainage basins are computed by error propagation from the thickness change rate errors, according to (22)

$$\sigma_{\Delta V,Total,Basin} = \sqrt{\sum_{i=1}^{N} \sigma^2_{\Delta h,total,Hvel,i} A^2_{Hvel,i} + \sum_{j=1}^{M} \sigma^2_{\Delta h,total,Lvel,j} A^2_{Lvel,j}} \qquad \textbf{[S4]}$$

where $\sigma_{\Delta h,total,Hvel,i}$ is the error of annual total ice thickness change rate in the dynamically active, high-velocity zone of the ice sheet (v > 50 m·y^{-1} from ref. 24) at location i; $A_{Hvel,i}$ is the area around location i; N is the number of elevation change rate reconstructions in the high-velocity zone; $\sigma_{\Delta h,total,Lvel,j}$ is the error of annual total ice thickness change rate in the dynamically inactive, low-velocity zone (v < 50 m y^{-1}) at location j; $A_{Lvel,j}$ is the area around location j; and M is the number of elevation change rate reconstructions in the low-velocity zone. We further simplify Eq. **S4** by setting $A_{Hvel} = A_{Hvel,1} = A_{Hvel,2} = \cdots = A_{Hvel,N}$ and $A_{Lvel} = A_{Lvel,1} = A_{Lvel,2} = \cdots = A_{Lvel,M}$ and by assuming that $\sigma_{Dh,total,Hvel} = \sigma_{\Delta h,total,Hvel,1} = \sigma_{\Delta h,total,Hvel,2} = \cdots = \sigma_{\Delta h,total,Hvel,N}$ and $\sigma_{\Delta h,total,Lvel} = \sigma_{\Delta h,total,Lvel,1} = \sigma_{\Delta h,total,Lvel,2} = \cdots = \sigma_{\Delta h,total,Lvel,M}$. With this, we obtain for the drainage basin volume change error:

$$\sigma^2_{\Delta V,Total,Basin} = \sigma^2_{\Delta h,total,Hvel} N A^2_{Hvel} + \sigma^2_{\Delta h,total,Lvel} M A^2_{Lvel} \qquad \textbf{[S5]}$$

$$= \sigma^2_{\Delta h,total,Hvel} \frac{A^2_{Basin,Hvel}}{N} + \sigma^2_{\Delta h,total,Lvel} \frac{A^2_{Basin,Lvel}}{M}$$

where $A_{Basin,Hvel}$ and $A_{Basin,Lvel}$ are the areas of high- and low-velocity portions, respectively, of the drainage basin.

Error of Annual Ice Dynamics-Related Volume Change Rate of Large Drainage Basins ($\sigma_{\Delta V,Dynamic,Basin}$). While errors of annual elevation changes can be assumed to be uncorrelated, errors of annual SMB-, firn compaction-, and ice dynamics-related ice thickness changes have large correlation lengths due to the inclusion of climate data (e.g., ref. 2). Therefore, we assume large errors, described below, for the SMB- and firn compaction-related volume and mass changes of the large drainage basins.

The error of the ice dynamics-induced volume change of large drainage basins is computed from the following errors by error propagation: the error of the total volume change of the basin estimated by Eq. **S5**; the error of the annual SMB anomaly-related volume change of the basin, estimated as 30% or at least 1 $km^3 \cdot y^{-1}$; and the error of the annual volume change related to changes in firn compaction velocity, estimated as 100% or at least 1 $km^3 \cdot y^{-1}$.

Error of Annual Total ($\sigma_{\Delta M,Total,Basin}$) and Ice Dynamics-Related ($\sigma_{\Delta M,Dynamic,Basin}$) Mass Change Rates of Large Drainage Basins. The error of the annual dynamic mass change rate of a drainage basin $(\sigma_{\Delta M,Dyn,Basin})$ is estimated as

$$\sigma_{\Delta M,Dyn,Basin} = 0.917\ \sigma_{\Delta V,Dyn,Basin}. \quad \text{[S6]}$$

Finally, the error of the annual total mass change of a drainage basin $(\sigma_{\Delta M,Basin})$ is estimated using the following equation:

$$\sigma_{\Delta M,Basin} = \sqrt{\sigma^2_{\Delta M,Dyn,Basin} + \sigma^2_{\Delta M,SMB,Basin} + \sigma^2_{misc,Basin}} \quad \text{[S7]}$$

where $\sigma_{\Delta M,SMB,Basin}$ is the error of annual SMB-related mass change rate of the drainage basin, assumed to be 30% or at least 1 $Gt \cdot y^{-1}$. Miscellaneous errors include the error caused by neglecting the effects of elastic crustal response to present ice mass changes as well as elevation changes due to subglacial melt. Based on estimates in ref. 19, we assume that σ_{misc} equals a total of 6 $G \cdot y^{-1}$ for the whole ice sheet, distributed to drainage basins according to their areas.

Classification of Outlet Glaciers According to Dynamic Behavior

Drainage of interior ice from the GrIS is accomplished through a network of tributaries and outlet glaciers. The most recent compilation of ice velocities over the GrIS identifies 242 outlet glaciers with a width exceeding 1.5 km (24). (Rignot and Mouginot list 243 glaciers. However, two glaciers, Kangilinnguata Sermia (ID = 165 in ref. 24) and Unnamed south bis Russell (ID = 166 in ref. 24) are at the same location.) Ice dynamical changes in these glaciers are, in part, responsible for the increase in mass loss from the GrIS. We used the dynamic thickness change histories to classify these outlet glaciers into different categories. Because we corrected the thickness change to remove thickness changes due to monthly SMB anomalies, our dynamic thickness change histories are not affected by seasonal elevation changes (Fig. S1, bottom row) and thus can be approximated by simple analytical functions. The detailed examination of our large "library" of ice sheet thickness change histories revealed that dynamic thinning or thinning of most outlet glaciers can be described by low-order polynomials (up to second-order) or sigmoid curves, fitted to the laser altimetry points (25). We approximate a sigmoid curve with the following equation:

$$h = \frac{-d(t-a)}{\sqrt{1+b(t-a)^2}} + c \quad \text{[S8]}$$

where t refers to time, h is relative elevation, and a, b, c, and d are the four parameters that describe the timing and magnitude of the dynamic thickness change event.

We established the following categories based on the best-fit analytical curves:

- Thinning or thickening: linear fit
- Accelerating or decelerating thinning: second-order polynomial fit
- Full cycle thinning: sigmoid fit
- Thinning/thickening/thinning with abrupt termination of initial thinning: piecewise polynomial
- Unique, e.g., periodic thickness change: piecewise polynomial.

The errors of the curve fitting parameters are determined by formal error propagation and used as an additional clue for categorizing outlet glacier behavior types. Taking the magnitude of the maximum and the annual thickness change rates into account, we developed the following final categories (Fig. 2 and Table S1):

- No dynamic change: linear fit with less than ± 0.5 $m \cdot y^{-1}$ average thickness change rate
- Slow thinning: linear fit with $[-5, -0.5]$ $m \cdot y^{-1}$ average thinning rate
- Rapid thinning: linear fit with larger than -5 $m \cdot y^{-1}$ average thinning rate
- Slow accelerating/decelerating thinning: second-order polynomial fit with $[-5, -0.5]$ $m \cdot y^{-1}$ average thinning rate
- Rapid accelerating/decelerating thinning: second-order polynomial fit with larger than -5 $m \cdot y^{-1}$ average thinning rate
- Slow full cycle thinning: sigmoid fit with smaller than -5 $m \cdot y^{-1}$ maximum annual thinning rate
- Rapid full cycle thinning: sigmoid fit with larger than -5 $m \cdot y^{-1}$ maximum annual thinning rate
- Slow thinning/thickening (ThinThick): initial thinning that abruptly terminated, followed by thickening, maximum annual thinning rate is smaller than -5 $m \cdot y^{-1}$
- Rapid thinning/thickening (ThinThick): initial thinning that abruptly terminated, followed by thickening, maximum annual thinning rate is larger than -5 $m \cdot y^{-1}$
- Slow thinning/thickening/thinning (ThinThickThin): initial thinning that abruptly terminated, followed by a short period of thickening and resumed thinning, maximum annual thinning rate is less than -5 $m \cdot y^{-1}$
- Rapid thinning/thickening/thinning (ThinThickThin): initial thinning that abruptly terminated, followed by a short period of thickening and resumed thinning, maximum annual thinning rate is larger than -5 $m \cdot y^{-1}$
- Thickening: linear fit with larger than 0.5 $m \cdot y^{-1}$ average thickening rate.

To divide the glaciers into different categories, two to five thickness change histories were examined along (or near) the central flow line of each glacier at different distances from the grounding line (marine-terminating glaciers) or from the location of maximum velocity (land-terminating glaciers). Glaciers exhibiting similar behaviors at all selected locations (Fig. S2 *A* and *B*) are classified according to the categories listed above. Surging glaciers can be recognized from the laser altimetry record based on their characteristic spatiotemporal dynamic thickness change patterns. For example, Størstrommen, L. Bistrup Bræ, and Marie Sophie glaciers (Fig. 2 and Fig. S2*C*), which are quiescent surging glaciers, show large, steady thickening at their source regions as ice accumulates upstream of the reduced flow, and thinning below the area where the surge was initiated, while the complex elevation change pattern of Hagen Bræ might indicate an ongoing surge (Table S1).

Dynamic thinning was negligible on 13 out of the 15 land-terminating glaciers (Tables S1 and S2). The exceptions are Qumanaarsuup Sermia and Nordensköld Glacier, where dynamic thinning might be associated with the dynamic thinning of neighboring marine-terminating outlet glaciers of Kangiata Nunaata Sermia and Jakobshavn Isbræ, respectively.

Our relatively sparse temporal sampling only allowed a qualitative characterization of rapid, short-term ice thickness variations. We considered the thickness change variation large when the fitting error of the analytical curve is larger than 0.3 m. We only applied this criterion on slowly changing glaciers (<2.5 $m \cdot y^{-1}$ thickness change rate). We detected large, short-term thickness variations, indicated as L in the column of ShortTerm of Table S1, on 15 glaciers, all marine terminating (Table S1). They may indicate control from subglacial hydrology or are perhaps related to the drainage of proglacial lakes (e.g., Daugaard-Jensen Glacier, Fig. S2*D*, ref. 26).

While the behavior of the four major outlet glaciers is similar to the dynamic patterns representative to their respective major drainage basin, the pattern of outlet glacier behavior varies significantly within the seven major drainage basins (Fig. 2*B* and Table S2). Moreover, the relative contribution of different drainage basins to the overall mass loss is not proportional to their area. For example, 47% of the total 2003–2009 mass loss originated from the southeast region (without Helheim and Kangerlussuaq glaciers), an area comprising only ∼10% of the ice sheet. All glaciers showing rapid abrupt thinning that terminated in 2005–2006 are found in southeast Greenland, but other, distinctively different glacier behavior, e.g., accelerating large thinning (Ikertivaq NN), is also detected in the same region. The outlet glaciers draining to the narrow fjords north of Jakobshavn Isbræ also show a complex spatial pattern of dynamic elevation changes (Fig. 2*B*, *Inset*). For example, glaciers terminating at the Torsukattak Fjord were thinning (Kangilerngata Sermia, Eqip Sermia), thickening (Sermeq Avannarleq), or exhibiting a complex behavior (Sermeq Kujalleq) during the same time period (Fig. 2*B*, *Inset*, and Table S1).

Comparison of SERAC Results to Previous Studies

Our average thinning rates are in good agreement with those published by Pritchard et al. (27) (Table S3), with an average difference of 0.3 ± 1.1 $m \cdot y^{-1}$ after the removal of one outlier (Helheim Glacier). However, a closer examination reveals other relatively large differences, especially for glaciers that are characterized by a nonlinear temporal thickness change pattern, e.g., Kangerlussuup Sermersua or Mælkejeven Glacier. Unlike SERAC, which reconstructs a complete temporal history of the elevation change, the method developed by Pritchard et al. (27) renders high spatial resolution along tracks at the cost of lower temporal resolution, providing a single elevation change rate only. Moreover, the selection of the observations contributing to a single elevation change rate is determined by the availability of good-quality ICESat observations within the region of interest and therefore somewhat arbitrary. We consider the two results to be in good agreement when the elevation change rates from Pritchard et al. (27) are within the bounds determined by the annual thickness change rates from this study. After applying this criterion, we identified two glaciers with larger than 1 $m \cdot y^{-1}$ difference (Table S3). The large difference on Zachariæ Isstrøm could be due to the different performance of the surface approximations used by the two studies over the crevassed surface near the grounding line. The comparison of the results over the thickening upstream regions of Storstrømmen and L. Bistrup Bræ glaciers suggests that the Pritchard et al. (27) study might systematically overestimate the thickening rates of surging glaciers, perhaps due to the simplified way it reconstructs the surface shape and its temporal evolution.

As Table S6 shows, our average GrIS and regional mass loss estimates agree well with previous studies (19, 28–37), with the exception of those that used satellite laser altimetry measurements only (the lower value in ref. 19, ref. 28) and the reconciled estimate derived from these studies by ref. 29. Including ATM and LVIS airborne laser altimetry observations allowed us to reconstruct the details of marginal thinning, resulting in a larger and more realistic thinning rate for the whole GrIS. We also found a good agreement between our regional average mass loss rates and those derived by refs. 30 and 32, showing that similar estimates are obtained using different firn compaction models (this study vs. ref. 30) or data sets [laser altimetry (this study) vs. GRACE (32)].

1. Cuffey KM, Patterson WSB (2010) *The Physics of Glaciers* (Elsevier, New York), 4th Ed.
2. Ettema J, van den Broeke MR, van Meijgaard E, van de Berg WJ, Bamber JL, Box JE, Bales RC (2009) Higher surface mass balance of the Greenland ice sheet revealed by high-resolution climate modeling. *Geophys Res Lett* 36(12):L12501.
3. van Angelen JH, van den Broeke MR, Wouters B, Lenaerts JTM (2014) Contemporary (1960–2012) evolution of the climate and surface mass balance of the Greenland ice sheet. *Surv. Geophys* 35(5):1155–1174.
4. Reeh N, Fisher DA, Koerner RM, Clausen HB (2005) An empirical firn-densification model comprising ice lenses. *Ann Glaciol* 42(1):101–106.
5. Reeh N (2008) A nonsteady-state firn-densification model for the percolation zone of a glacier. *J Geophys Res* 113(F3):F03023.
6. Rastner P, Bolch T, Molg N, Machguth H, Paul F (2012) The first complete glacier inventory for the whole of Greenland. *Cryosphere* 6(6):1483–1495.
7. Zwally HJ, et al. (2011) *GLAS/ICESat L2 Antarctic and Greenland Ice Sheet Altimetry Data V33* (Natl Snow Ice Data Cent, Boulder, CO).
8. Borsa AA, Moholdt G, Fricker HA, Brunt KM (2014) A range correction for ICESat and its potential impact on ice-sheet mass balance studies. *Cryosphere* 8(2):345–357.
9. Urban T, et al. (2012) Summary of ICESat-1 inter-campaign elevation biases and detection methods. *Eos Trans AGU* 93(52, Fall Meet Suppl):abstr C13H-03.
10. Smith BE, Fricker HA, Joughin IR, Tulaczyk S (2009) An inventory of active subglacial lakes in Antarctica detected by ICESat (2003–2008). *J Glaciol* 55(192):573–595.
11. Fricker HA, et al. (2005) Assessment of ICESat performance at the salar de Uyuni, Bolivia. *Geophys Res Lett* 32(21):L21S06.
12. Shuman CA, et al. (2006) ICESat Antarctic elevation data: Preliminary precision and accuracy assessment. *Geophys Res Lett* 33(7):L07501.
13. Krabill WB (2014) *IceBridge ATM L2 Icessn Elevation, Slope, and Roughness* (Natl Snow Ice Data Cent, Boulder, CO), Version 2.
14. Krabill WB, et al. (2002) Aircraft laser altimetry measurement of elevation changes of the Greenland ice sheet: Technique and accuracy assessment. *J Geodyn* 34(3):357–376.
15. Martin CF, Krabill WB, Manizade SS, Russell RL (2012) *Airborne Topographic Mapper Calibration Procedures and Accuracy Assessment* (NASA Goddard Space Flight Cent, Greenbelt, MD), Tech Memo 2012-215891.
16. Blair JB, Hofton M (2014) *IceBridge LVIS L2 Geolocated Surface Elevation Product* (Natl Snow Ice Data Cent, Boulder, CO).
17. Hofton MA, Blair JB, Luthcke SB, Rabine DL (2008) Assessing the performance of 20-25 m footprint waveform lidar data collected in ICESat data corridors in Greenland. *Geophys Res Lett* 35(24):L07501.
18. A G, Wahr J, Zhong S (2013) Computations of the viscoelastic response of a 3-D compressible Earth to surface loading: An application to Glacial Isostatic Adjustment in Antarctica and Canada. *Geophys J Int* 192(2):557–572.
19. Sørensen LS, Simonsen SB, Nielsen K, Lucas-Picher P, Spada G, Adalgeirsdottir G, Forsberg R, Hvidberg CS (2011) Mass balance of the Greenland ice sheet (2003–2008) from ICESat data—The impact of interpolation, sampling and firn density. *Cryosphere* 5(1):173–186.
20. Lucas-Picher P, et al. (2012) Very high-resolution regional climate model simulations over Greenland: Identifying added value. *J Geophys Res* 117(D2):D02108.
21. Vernon CL, et al. (2013) Surface mass balance model intercomparison for the Greenland ice sheet. *Cryosphere* 7(2):599–614.
22. Schenk T, Csathó B (2012) A new methodology for detecting ice sheet surface elevation changes from laser altimetry data. *IEEE Trans Geosci Remote Sens* 50(2):3302–3316.
23. Koch KR (1999) *Parameter Estimation and Hypothesis Testing in Linear Models* (Springer, Berlin).
24. Rignot E, Mouginot J (2012) Ice flow in Greenland for the International Polar Year 2008–2009. *Geophys Res Lett* 39(11):L11501.
25. Schenk T, Csatho B, van der Veen C, McCormick D (2014) Fusion of multi-sensor surface elevation data for improved characterization of rapidly changing outlet glaciers in Greenland. *Remote Sens Environ* 149:239–251.
26. Reeh N, Olesen OB (1986) Velocity measurements on Daugaard-Jensen Gletscher, Scoresby Sund, East Greenland. *Ann Glaciol* 8:146–150.
27. Pritchard HD, Arthern RJ, Vaughan DG, Edwards LA (2009) Extensive dynamic thinning on the margins of the Greenland and Antarctic ice sheets. *Nature* 461(7266):971–975.
28. Zwally HJ, et al. (2011) Greenland ice sheet mass balance: Distribution of increased mass loss with climate warming; 2003-07 versus 1992–2002. *J Glaciol* 57(201):88–102.
29. Shepherd A, et al. (2012) A reconciled estimate of ice-sheet mass balance. *Science* 338(6111):1183–1189.
30. Sasgen I, et al. (2012) Timing and origin of recent regional ice-mass loss in Greenland. *Earth Planet Sci Lett* 333:293–303.
31. Khan SA, et al. (2014) Sustained mass loss of the northeast Greenland ice sheet triggered by regional warming. *Nat Clim Change* 4(4):292–299.
32. Chen JL, Wilson CR, Tapley BD (2011) Interannual variability of Greenland ice losses from satellite gravimetry. *J Geophys Res* 116(B7):B07406.
33. Luthcke SB, et al. (2013) Antarctica, Greenland and Gulf of Alaska land-ice evolution from an iterated GRACE global mascon solution. *J Glaciol* 59(216):613–631.

34. Enderlin EM, et al. (2014) An improved mass budget for the Greenland ice sheet. *Geophys Res Lett* 41(3):866–872.
35. Rignot E, Velicogna I, van den Broeke MR, Monaghan A, Lenaerts J (2011) Acceleration of the contribution of the Greenland and Antarctic ice sheets to sea level rise. *Geophys Res Lett* 38(5):L05503.
36. van den Broeke M, et al. (2009) Partitioning recent Greenland mass loss. *Science* 326(5955):984–986.
37. Kjeldsen KK, et al. (2013) Improved ice loss estimate of the northwestern Greenland Ice Sheet. *J Geophys Res* 118(2):698–708.

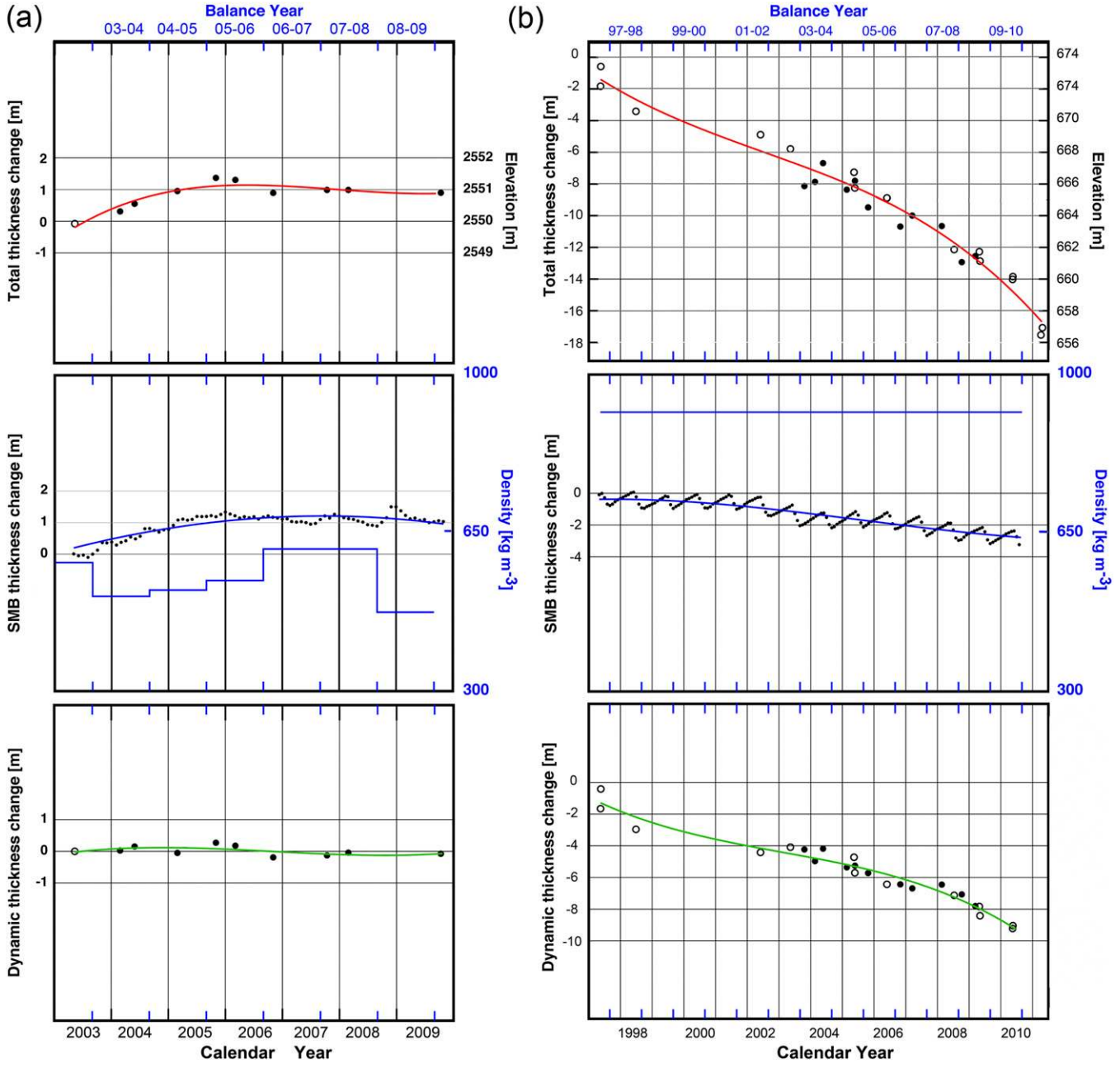

Fig. S1. Examples of elevation change histories derived from ICESat and ATM data using SERAC: (*A*) near the ice divide in south Greenland (negligible ice motion) and (*B*) over Sermeq Avannarleq in west Greenland ($v \approx 60$ m·y^{-1}). Locations are marked in Fig. 1. *Upper* shows thickness change reconstructed by SERAC as a function of time. Filled circles mark data ICESat crossovers, and empty circles mark data derived by combining ICESat with ATM airborne laser altimetry. *Middle* shows monthly thickness changes related to SMB anomalies (black dots) and the estimated density of the annual surface firn layer (blue curve). *Lower* shows calculated dynamic thickness changes. Red, blue, and green curves are the polynomial approximations of the total, SMB-related, and ice dynamics-related thickness changes, respectively.

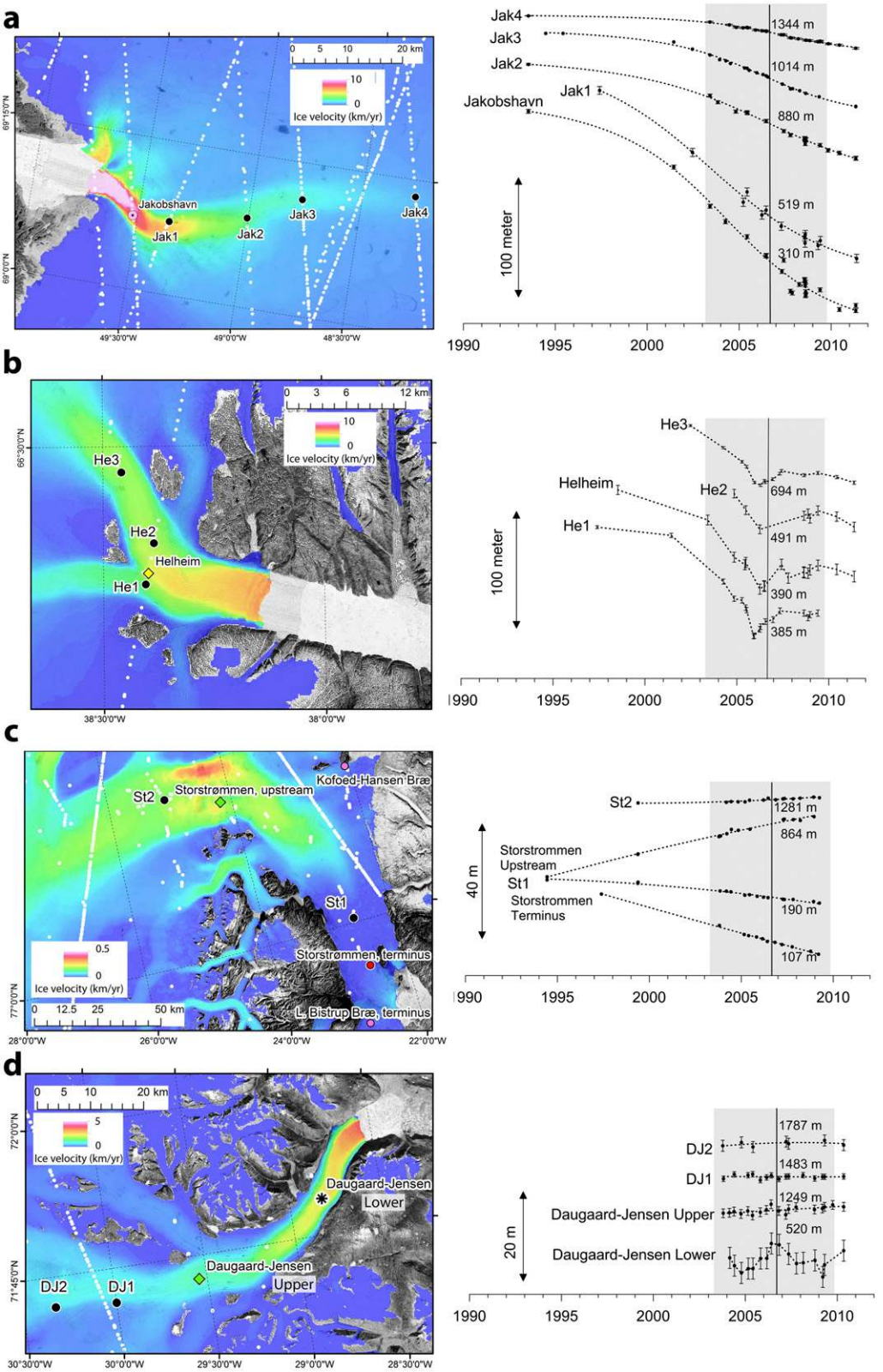

Fig. S2. Illustration of dynamic elevation adjustment patterns. (*A*) Jakobshavn Isbræ—full cycle thinning: thinning propagating upstream with its onset and termination detected. (*B*) Helheim Glacier—abrupt: abrupt termination of thinning followed by thickening. (*C*) Storstrømmen Glacier—contrasting elevation changes in the upper and lower drainage basin as the glacier is recovering from a surge. (*D*) Daugaard Jensen Glacier—cyclic, rapid elevation changes of the Daugaard Jensen Lower site are likely related to periodic filling and drainage of a large proglacial lake located 5 km west. Such a drainage event, causing the uplift of the surface, was observed in 1968 and reported by ref. 26. Thickness change curves are reconstructed from ICESat, ATM, and LVIS laser altimetry observations. Gray shaded area marks the duration of the ICESat mission, and numbers show glacier surface elevations on August 31, 2006. Locations of thickness change curves are shown on a combination of Landsat imagery (b/w) and ice flow velocity from ref. 24 (color).

Fig. S3. (*A*) Annual mass change rates associated with ice dynamics for the four major glaciers and seven major drainage basins. The southeast (SE), Jakobshavn (Jak), and North (N) drainage basins are divided into main outlet glaciers [Helheim (He), Kangerlussuaq (Ka), Jakobshavn Isbræ (JI), and Petermann (Pet)] and the rest [SE Rest, Jak Rest, N Rest]. HKJP is the total annual mass loss of the four major glaciers, and GrIS Rest shows the contribution from the rest of the GrIS. (*B*) Relative area of major glaciers and drainage basins exhibiting mass loss in 2003–2009 and their contribution to the overall GrIS mass loss.

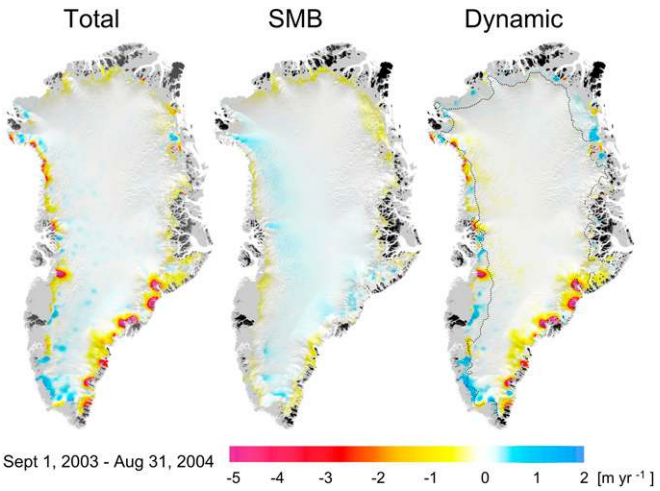

Movie S1. Annual total, SMB-related, and ice dynamics-related thickness change rates of the GrIS for 2003–2009 balance years from ICESat, ATM, and LVIS laser altimetry observations. Dotted lines on the dynamic thickness change maps mark the ELA (average 2003–2009 SMB = 0). Ice sheet boundary is from ref. 6, and black regions show weakly or not connected glaciers and ice caps. See Fig. 1*D* for locations of the elevation change time series.

Movie S1

Other Supporting Information Files

Table S1 (PDF)
Table S2 (PDF)
Table S3 (PDF)
Table S4 (PDF)
Table S5 (PDF)
Table S6 (PDF)

Table S1. Dynamic thickness change patterns of GrIS outlet glaciers based on: (i) their entire record and (ii) during the ICESat mission period (2003-2009). See Fig. 2*A* for elevation change histories illustrating different thickness change pattern types, and Fig. 2*B* for spatial distribution of different outlet glacier types.

Glacier [a]	ID	Region	Type	SERAC Solution		Dist. [b]	Record	Dynamic thickness change pattern				Note
				Lat	Lon		Span	Entire Record	2003-09 Record			
				(deg)	(deg)	(km)		Type	Type	MaxRate[c]	ShortTerm[d]	
Jakobshavn Isbræ	1	Jak	TW	69.1192	-49.5236	6.9	1993-2012	Full cycle thinning	Thinning	R		
Kangerlussuaq	2	SE	TW	68.7671	-33.3509	23.5	1998-2012	Full cycle thinning	Full cycle thinning	R		
Helheim	3	SE	TW	66.3851	-38.3983	8.5	1998-2012	ThinThickThin	ThinThick	R		
Køge Bugt C	4	SE	TW	65.1781	-41.1141	2.5	2004-2011	ThinThickThin	ThinThickThin	R		*Shear zone*
Rink Isbræ	5	Jak	TW	71.7937	-51.1943	14.9	1993-2011	Full cycle thinning	Thinning	R		
Store	6	Jak	TW	70.4370	-50.393	7.1	2003-2012	Thickening	Thickening			
Gyldenløve Fjord C	7	SE	TW	64.2331	-41.5429	2.6	2004-2009	Thinning	Thinning	R		*Shear zone*
Daugaard-Jensen	8	E	TW	71.8108	-28.8236	13.5	2004-2011	Unique	Unique, periodic		L	*Lake drainage?*[e]
Uunartit Islands* [f]	10	SE	TW	67.3891	-33.9403	18.3	2004-2012	Thinning	Thinning	S		
Deception Ø CN*	11	SE	TW	67.7590	-33.9430	27.6	2003-2012	Thinning	Thinning	S		
A.P. Bernstorff	12	SE	TW	63.8491	-41.7052	1.6	2004-2012	ThinThickThin	ThinThickThin	R		
Sermeq Kujalleq	13	Jak	TW	69.9890	-50.1234	2.0	1997-2012	ThinThickThin	Unique, ThickThin	S	L	
Køge Bugt S	14	SE	TW	65.0024	-41.1958	2.3	2004-2011	ThinThickThin	ThinThick	R	L	
Tingmiarmiut Fjord	15	SE	TW	62.7937	-43.4355	7.6	1998-2008	Full cycle thinning	Full cycle thinning	R		
Kong Oscar	16	NW	TW	76.0672	-59.5151	7.4	1999-2012	Full cycle thinning	Full cycle thinning	S		
Alison	17	NW	TW	74.7071	-55.6495	16.5	2004-2012	Thinning	Thinning	S		
Upernavik Isstrøm C	18	NW	TW	73.0566	-53.5796	27.0	2003-2009	Accelerating thinning	Accelerating thinning	S		
Graulv	19	SE	TW	64.3496	-41.4914	2.3	2004-2009	Full cycle thinning	Full cycle thinning	S		
Ukaasorsuaq	20	SW	TW	62.0292	-48.3002	23.5	2003-2011	Thickening	Thickening			
Illullip Sermia	21	NW	TW	74.3980	-55.9834	2.1	2004-2010	Thinning	Thinning	S		
Upernavik Isstrøm S	22	NW	TW	72.8282	-53.8742	14.6	1999-2011	Thinning	Thinning	S		
Mogens Heinesen S*	23	SE	TW	62.3373	-43.1271	0.7	2004-2012	Decelerating thinning	Decelerating thinning	R		
S Hayes M*	24	NW	TW	74.8320	-56.3102	9.0	2004-2012	Thinning	Thinning	S		
Sermeq Silarleq	25	Jak	TW	70.8910	-50.7144	8.3	2003-2012	Thinning	Thinning	S		
Upernavik Isstrøm N	26	NW	TW	73.0072	-54.4216	11.1	2003-2010	Thinning	Thinning	R		*Retreated by '08*
Steenstrup	27	NW	TW	75.2983	-57.8939	1.2	2003-2012	Thinning	Thinning	R		
Sverdrup	28	NW	TW	75.5933	-58.1019	1.5	2003-2010	Decelerating thinning	Decelerating thinning	R		
Qajuuttap Sermia	30	SW	TW	61.4114	-45.6105	7.9	2004-2012	Thickening	Thickening		L	
K.I.V.S. Nodre Bræ[g]	35	SE	TW	66.6607	-35.0927	30.1	2003-2012	No dynamic change	No dynamic change			
Kangiata Nunaata S.	36	SW	TW	64.1734	-49.3330	14.7	1998-2012	Full cycle thinning[h]	ThinThick	S		
Hayes	37	NW	TW	74.9807	-56.8436	7.4	2003-2012	Accelerating thinning	Accelerating thinning	S	L	*Onset*
Frederiksborg	38	SE	TW	68.3124	-31.4985	6.2	2003-2012	Thinning	Thinning	S		
Heimdal	39	SE	TW	62.8991	-42.6795	5.3	2003-2012	Thickening	Thickening		L	
Kakivfaat Sermiat	41	NW	TW	73.4841	-55.2759	4.8	2003-2012	Accelerating thinning	No dynamic change	S		
Kong Christian IV	42	SE	TW	68.5554	-30.3101	21.3	1993-2012	No dynamic change	No dynamic change			
Herluf Trolle N*	43	SE	TW	61.3060	-43.5238	10.7	2004-2012	ThinThickThin	ThinThick	R		
Herluf Trolle S*	45	SE	TW	61.2229	-43.5538	13.3	1998-2011	Full cycle thinning	Thinning	S		
Ikertivaq NN	46	SE	TW	65.7225	-39.6796	5.0	1997-2008	Accelerating thinning	Accelerating thinning	R		
Kangerlussuup S.[i]	47	Jak	TW	71.4254	-50.6849	22.9	1993-2011	No dynamic change	No dynamic change			
Vestfjord	48	E	TW	70.3073	-29.4262	11.8	1998-2011	No dynamic change	No dynamic change			
Fenris	49	SE	TW	66.3992	-37.5917	4.3	2003-2012	ThinThickThin	ThinThickThin	R		
Køge Bugt N	50	SE	TW	65.2313	-40.7742	4.9	2004-2011	ThinThickThin	ThinThick	R		

[a] Glacier names, IDs and glacier types are from ref. 24. Glacier names mentioned in this study are in bold.
[b] Distance from calving front (marine glaciers) or from velocity maximum (land-terminating glaciers) as listed in ref. 24.
[c] MaxRate: maximum annual thinning rate in 2003-2009, R (Rapid) is larger than -5 m $\cdot y^{-1}$, S (Slow) is smaller than -5 m $\cdot y^{-1}$.
[d] ShortTerm: large ice thickness variations over short time periods.
[e] Rapid drainage of a proglacial lake located 5 km west of this site was observed in 1968 (26).
[f] * marks glacier names starting with "unnamed" in ref. 24.
[g] K.I.V. Steenstrup Nodre Bræ.
[h] Abrupt thickening at the termination of the full cycle thinning.
[i] Kangerlussuup Sermersua.

Glacier	ID	Region	Type	SERAC Solution		Dist,	Record	Dynamic thickness change pattern				Note
				Lat	Lon		Span	Entire Record	2003-09 Record			
				(deg)	(deg)	(km)		Type	Type	MaxRate	ShortTerm	
Zachariae Isstrøm	51	NE	TW	78.9071	-20.8642	7.1	1994-2012	Accelerating thinning	Thinning	S		
Kangilerngata S.	52	Jak	TW	69.9204	-50.2788	3.5	2005-2012	Thinning	Thinning	S		
Sermeq Avannarleq	53	Jak	TW	70.1069	-50.1683	7.7	2003 -2012	Thickening	Thickening		L	
kertivaq M	54	SE	TW	65.6176	-40.1091	4.7	2004-2012	No dynamic change	No dynamic change		L	
Kruuse Fjord	57	SE	TW	67.2117	-33.8403	1.6	2004-2009	Thinning	Thinning	R		
Rimfaxe	58	SE	TW	63.2500	-42.2939	4.4	2003-2011	Thickening	Thickening			
Tracy	59	NW	TW	77.6587	-65.7384	9.2	2003-2011	Thinning	Thinning	R		
Mogens Heinesen C*	60	SE	TW	62.4476	-43.2980	13.2	2003-2011	Thinning	Thinning	S		*Not on fast flow*
Polaric	61	SE	TW	67.9937	-32.4782	12.7	2003-2012	No dynamic change	No dynamic change			
Narsap Sermia	63	SW	TW	64.7208	-49.5757	23.1	2003-2012	Accelerating thinning	Thinning	S		
Gyldenløve Fjord S	64	SE	TW	64.1679	-41.5667	4.0	2004-2009	Decelerating thinning	Decelerating thinning	R		
Qooqqup Sermia	66	SW	TW	61.4027	-44.8172	29.7	2004-2012	Thinning	Thinning	S		
Umiammakku Isbræ	68	Jak	TW	71.7365	-52.4101	1.0	2003-2012	Full cycle thinning	Full cycle thinning	R		
Heilprin	70	NW	TW	77.5280	-65.9561	1.9	2003-2011	Thinning	Thinning	S		
Mælkevejen	73	SE	TW	63.6930	-41.6810	3.8	2004-2008	Decelerating thinning	Thinning	R		
79North[a]	74	NE	TW	79.3423	-22.6087	1.4	1999-2009	No dynamic change	No dynamic change			
Dietrichson	75	NW	TW	75.4585	-57.9395	1.6	2004-2012	Accelerating thinning	Thinning	S		
Eqalorutsit K S[b]	76	SW	TW	61.3361	-46.4358	14.4	2004-2011	Thinning	Thinning	S		
Petermann	78	N	TW	80.5037	-60.0385	7.6	1994-2011	No dynamic change	No dynamic change			
Polaric S*	80	SE	TW	67.8080	-33.3190	5.2	2005-2012	Decelerating thinning	Decelerating thinning	S		
Skinfaxe	82	SE	TW	63.2996	-41.9407	4.0	2004-2011	Thickening	Thickening			
Kjer	83	NW	TW	75.1365	-57.5483	7.4	2004-2012	Thinning	Thinning	S		
Kanger W*	87	SE	TW	68.5156	-33.2014	11.7	2003-2010	Decelerating thinning	Decelerating thinning	R		
Inngia Isbræ	88	Jak	TW	72.1210	-52.4739	10.9	2003-2012	Accelerating thinning	Thinning	S		
Docker Smith W	89	NW	TW	76.3351	-61.8923	0.7	1999-2011	Decelerating thinning	Thinning	R		
Eqip Sermia	90	Jak	TW	69.7704	-49.9416	11.7	2003-2012	Thinning	Thinning	S		
Storbræ N	93	SE	TW	68.9585	-26.0292	3.7	2003-2011	Decelerating thinning	Decelerating Thinning	R		
Gerard de Geer	94	E	TW	73.6986	-27.4391	22.3	2003-2012	No dynamic change	No dynamic change			
Issuuarsuit Sermia	97	NW	TW	76.1758	-60.4427	15.2	1999-2010	Accelerating thinning	Thinning	S		
Docker Smith	100	NW	TW	76.3319	-61.4529	12.7	2003-2010	Thinning	Thinning	S		
Qeqertarsuup Sermia	101	NW	TW	73.5977	-55.4656	2.9	2003-2012	Accelerating thinning	Thinning	S		
Kronborg	102	SE	TW	68.4526	-28.6509	5.9	2003-2012	Decelerating thinning	Thinning	R		
S Hayes SS*	105	NW	TW	74.7549	-56.3935	6.2	2004-2010	Thinning	Thinning	R		
Ussing Brær N	106	NW	TW	73.9718	-55.6199	4.8	2003-2012	Thinning	Thinning	S	L	
N Oscar S*[c]	107	NW	TW	76.0962	-59.8199	8.8	2003-2010	Accelerating thinning	Accelerating thinning	S		
Danell Fjord*	108	SE	TW	60.9209	-43.6656	6.6	2004-2012	Thickening	Thickening			
Hagen Bræ	111A	NE	TW	81.4164	-27.7163	3.7	1994-2011	ThinThickenThin	Thickening			*closest to terminus*
Hagen Bræ	111B	NE	TW	81.4029	-27.8820	6.6	1994-2011	ThickenThin	Thinning	S		*upstream from 111A*
Hagen Bræ	111C	NE	TW	81.3441	-28.8902	24.2	2004-2011	Decelerating thinning	Decelerating thinning	R		*upstream from 111B*
Akullersuup Sermia	115	SW	TW	64.3981	-49.4339	8.0	2003-2012	No dynamic change	No dynamic change			
Hayes N	116	NW	TW	75.0556	-57.3808	7.9	2003-2012	Thinning	Thinning	S	L	
Carlos	118	NW	TW	76.5938	-63.6556	20.0	2003-2012	Thinning	Thinning	S		
Midgård	121	SE	TW	66.4960	-36.74	10.0	2004-2012	Thinning, varying rate	Decelerating thinning	R		
Glacier de France	127	SE	TW	66.5138	-36.2063	14.8	2003-2012	Thinning	Thinning	S		
Cornell	130	NW	TW	74.2471	-56.0375	1.5	2003-2010	Thinning	Thinning	S		
Kista Dan	132	E	TW	69.9523	-27.4633	1.5	2003-2012	No dynamic change	No dynamic change			
Humboldt	139	N	TW	79.7446	-63.9700	7.4	1997-2009	Thinning	Thinning	S		
Frederikshåbs Isblink	141	SW	LT	62.7241	-49.6221	7.1	2003-2011	No dynamic change	No dynamic change			
S Danell Fjord*	143	SE	TW	60.8439	-43.6930	3.9	2004-2012	Decelerating thinning	Thinning	S		
Ryder	144	N	TW	81.5074	-50.3701	4.1	1997-2011	Thinning	Thinning	S		
S Russell*	148	SW	LT	67.0199	-49.9078	3.2	1998-2011	No dynamic change	No dynamic change			*Maximum velocity*
Carlos W	151	NW	TW	76.4116	-63.6883	4.6	2004-2010	Thinning	Thinning	S		
Vestfjord S*	157	E	TW	69.9325	-28.2497	13.2	2003-2011	No dynamic change	No dynamic change		L	
Steenby glacier	159	N	TW	81.4431	-54.0752	6.3	1999-2011	No dynamic change	No dynamic change			
Academy	163	N	TW	81.4539	-32.3670	19.4	2003-2009	Accelerating thinning	Accelerating thinning	S		
Kangilinnguata S.	165	SW	LT	64.965	-49.687	8.6	2003-2011	No dynamic change	No dynamic change			*Upstream of max vel*
Courtauld	167	SE	TW	68.5127	-32.1764	1.4	2003-2012	Thinning	Thinning	S	L	

[a] Nioghalvfjerdsfjorden.

[b] Eqalorutsit Killit Sermiat.

[c] Not in ref. 24, located between Kong Oscar and N Oscar.

Glacier	ID	Region	Type	SERAC Solution		Dist,	Record	Dynamic thickness change pattern				Note
				Lat	Lon		Span	Entire Record	2003-09 Record			
				(deg)	(deg)	(km)		Type	Type	MaxRate	ShortTerm	
Saqqarliup Sermia	168	Jak	TW	68.8981	-50.2935	1.3	2001-2011	Accelerating thinning	Thinning	S		
Brikkerne	169	N	TW	81.8183	-45.4605	2.5	2003-2009	No dynamic change	No dynamic change			
Qamanaarsuup S.	173	SW	LT	64.4845	-49.4714	1.1	2003-2011	Decelerating thinning	Thinning	S	L	*Maximum velocity*
Harder	177	N	TW	81.6158	-44.6664	5.3	2003-2009	No dynamic change	No dynamic change			
South of Sermeq	178A	SW	LT	63.6276	-49.2491	3.6	2003-2011	No dynamic change	No dynamic change			*Maximum velocity*
South of Sermeq	178B	SW	LT	63.5168	-49.5842	17.5	2004-2011	Thinning	Thinning			*Terminus*
Helland E	179	NW	TW	76.3443	-64.8030	8.4	2003-2009	No dynamic change	No dynamic change			
Nakkaasorsuaq	181	SW	TW	63.0757	-49.4791	10.7	2004-2011	No dynamic change	No dynamic change			
Majorqaq	182	SW	LT	65.7595	-50.0658	10.7	2004-2011	No dynamic change	No dynamic change			*Upstream of max vel*
Usulluup Sermia	183	SW	LT	68.0024	-50.0266	6.7	2004-2012	No dynamic change	No dynamic change			*Upstream of max vel*
Jætte	185	E	TW	73.4483	-27.6804	1.4	2003-2009	Thickening	Thickening			
Nordenskiöld	188	SW	LT	68.3927	-50.5976	4.3	2003-2011	Thinning	Thinning	S		*Upstream of max vel*
Saqqap Sermersua	189A	SW	LT	65.3044	-50.3826	2.3	1993-2011	No dynamic change	No dynamic change			*Maximum velocity*
Saqqap Sermersua	189B	SW	LT	65.2113	-50.6708	14.8	2004-2012	Decelerating thinning	Thinning			*Terminus*
Wordie	190A	E	LT	74.5106	-23.8801	1.7	1997-2009	No dynamic change	No dynamic change			*Maximum velocity*
Wordie	190B	E	LT	74.1752	-22.4369	57.2	1994-2008	ThickenThin	Thinning	S		*Terminus*
Kangerluarsuup S.	191	Jak	TW	71.2100	-50.9589	19.4	2003-2012	Thinning	Thinning	S		
Morell	193	NW	TW	76.3418	-62.4143	7.7	2003-2011	Full cycle thinning	Full cycle thinning	S		
Nordenskiöld	194	E	TW	73.1316	-27.9783	2.7	2003-2012	ThinThickenThin	ThinThicken	S	L	
Kangaasarsuup S.	197A	SW	LT	64.0409	-49.2762	13.1	2003-2011	No dynamic change	No dynamic change			*Maximum velocity*
Kangaasarsuup S.	197B	SW	LT	64.1491	-49.8221	16.2	2003-2009	Accelerating thinning	Accelerating thinning	S		*Terminus*
Violin	200A	E	LT	72.372	-27.0499	2.1	2003-2012	No dynamic change	No dynamic change			*Maximum velocity*
Violin	200B	E	LT	72.1545	-26.6988	28.2	2003-2012	Thinning	Thinning	S		*Terminus*
Isunnguata Sermia	205	SW	LT	67.1855	-49.9966	0.2	2003-2010	No dynamic change	No dynamic change			*Maximum velocity*
Russell	212	SW	LT	67.0997	-49.9542	0.6	1993-2011	No dynamic change	No dynamic change			*Maximum velocity*
Waltershausen	214	E	TW	73.843	-24.366	5.2	1997-2009	Accelerating thinning	Thinning	S		
Wahlenberg	215	E	LT	72.6218	-27.9065	6.3	2003-2012	No dynamic change	No dynamic change			*Maximum velocity*
Helland	216	NW	TW	76.2987	-64.8649	12.1	2003-2009	No dynamic change	No dynamic change			
Marie Sophie	217A	N	TW	81.7733	-33.1402	4.4	2003-2009	Thinning	Thinning	S		*Terminus*
Marie Sophie	217B	N	TW	81.8191	-33.7598	14.7	2003-2009	Thickening	Thickening			*Upstream*
Alangorliup Sermia	219	Jak	TW	68.9139	-50.1742	4.0	1997-2011	ThickenThin	Thinning	S		
Harald Moltke Bræ	220	NW	TW	76.5695	-67.6300	5.6	2004-2011	Thinning	Thinning	S	L	
Storstrømmen	225A	NE	TW	76.8391	-22.5615	14.7	1997-2012	Thinning	Thinning	S		*Terminus*
Storstrømmen	225B	NE	TW	77.5358	-24.1853	102.3	1994-2008	Thickening	Thickening			*Upstream*
Eielson	230	E	TW	71.1735	-28.0054	6.1	2003-2011	Thinning	Thinning	S		
Nordfjord	233	SE	TW	68.6567	-32.6238	1.2	2003-2012	Thinning	Thinning	S		
Pitugfik	234	NW	TW	76.2768	-68.5562	9.7	2003-2011	Accelerating thinning	Thinning	S		
Kofoed-Hansen Bræ	240	NE	TW	77.5141	-21.8244	1.6	2003-2012	Thinning	Thinning	S		
Newman Bugt	241	N	TW	81.2588	-57.1194	8.5	2003-2012	No dynamic change	No dynamic change			
L. Bistrup Bræ	242A	NE	TW	76.6414	-22.8038	2.8	1994-2009	Accelerating thinning	Thinning	S		*Terminus*
L. Bistrup Bræ	242B	NE	TW	76.2284	-22.9404	46.6	1997-2012	Thickening	Thickening			*Upstream*

Table S2. Distribution of outlet glaciers exhibiting different dynamic behaviors in 2003-2009 (Table S1) within the major drainage basins shown in Fig. 2*B*. Bold letters mark the most common outlet glacier behavior type in each drainage basin according to the number of glaciers and to the total drainage area.

		North		Northeast		East		Southeast		Southwest		Jakobshavn		Northwest		GrIS	
Category	Type	N[a]	Area [b] [km^2]	N	Area [km^2]	N	Area [km^2]	N	Area [km^2]	N	Area [km^2]	N	Area [km^2]	N	Area [km^2]	N	Area [km^2]
Slow thinning	TW	2	77098	1	2231	2	18411	**11**	17914	2	9102	**8**	63518	**18**	**114437**	44	302711
Rapid thinning	TW	0	0	0	0	0	0	2	4792	0	0	1	**90135**	5	41243	8	136170
Slow accelerating thinning	TW	1	25279	1	95103	0				1	2013	0	0	3	22733	6	145128
Rapid accelerating thinning	TW	0	0	0	0	0	0	1	2197	0	0	0	0	0	0	1	2197
Slow decelerating thinning	TW	0	0	0	0	1	550	0	0	0	0	0	0	0	0	1	550
Rapid decelerating thinning	TW	0	0	0	0	0	0	5	6661	0	0	0	0	1	12625	6	18736
Slow full cycle thinning	TW	0	0	0	0	0	0	1	6238	0	0	0	0	2	23597	3	29835
Rapid full cycle thinning	TW	0	0	0	0	0	0	2	**99955**	0	0	1	2296	0	0	3	102251
Thickening	TW	0	0	0	0	1	10833	4	8865	1	5398	2	38267	0	0	8	63363
Slow thinning-thickening	TW	0	0	0	0	1	4570	0	0	1	19583	0	0	0	0	2	24153
Rapid thinning-thickening	TW	0	0	0	0	0	0	4	56478	0	0	0	0	0	0	4	53478
Rapid thinning-thickening-thinning	TW	0	0	0	0	0	0	3	27644	0	0	0	0	0	0	3	27644
No dynamic change	TW	**5**	**80185**	1	**103278**	**5**	27306	3	11354	3	18977	1	4979	2	325	20	246404
Unique behavior	TW	0	0	0	0	1	**49230**	0	0	0	0	1	20667	0	0	2	69897
Surge	TW	1	3539	**3**	89954	0	0	0	0	0	0	0	0	0	0	4	93493
Thinning	LT	0	0	0	0	0	0	0	0	2	15314	0	0	0	0	2	15314
No dynamic change	LT	0	0	0	0	3	20549	0	0	**10**	**92620**	0	0	0	0	12	113169
Glaciers investigated in this study		9	186101	6	290566	14	131449	36	241548	20	163007	14	219862	31	214960	130	1447493
>1.5 km wide glaciers[c]		12		13		21		81		33		18		64		**242**	
Total area of region, this sudy			199240		365060		170464		260988		228136		221672		271776		1717336
% of glaciers/area, this study		75	**93**	46	**80**	67	**77**	44	**93**	61	**71**	78	**99**	48	**79**	54	**84**

[a]Number of glaciers.

[b]Combined area of drainage basins, from ref. 24.

[c]From ref. 24. The authors list 243 glaciers. However, two glaciers, Kangilinnguata Sermia (165) and Unnamed south bis Russell (166) are at the same location.

Table S3. Comparison of average, minimum and maximum thickness change rates during the 2003 February-2007 November period from SERAC (this study) and from Pritchard et al. (27).

Glacier name [a]	This study							Pritchard et al., 2009				Distance[b]
	ID	Lat.	Lon.	h (m) [c]	dh/dt ($m \cdot y^{-1}$)			Lat.	Lon.	h (m)	dh/dt [d]	(km)
					Min.	Max.	Ave.				($m \cdot y^{-1}$)	
Jakobshavn Isbræ lower	1	69.10964	-49.3630	515	–14.1	-11.8	**–13.1**	69.10300	-49.3684	490	**-13.1**	0.7
Jakobshavn Isbræ upstream	1	69.20985	-48.2504	1346	–3.5	-3.0	**-3.3**	69.21365	-48.2395	1350	**-3.5**	0.6
Kangerlussuaq Glacier	2	68.67335	-33.2939	825	-17.4	-7.1	**-14.1**	68.68163	-33.2890	840	**-17.7**	1.0
Helheim Glacier	3	66.37228	-38.4052	375	-36.1	9.0	**-13.8**	66.35129	-38.3681	340	**-23.0**	2.9
Rink Isbræ	5	71.77396	-50.5997	1102	-1.2	-0.8	**-0.9**	71.77852	-50.5857	1070	**-1.0**	0.5
Kong Oscar Glacier	16	76.06704	-59.5222	418	-2.9	-1.9	**-2.3**	76.06851	-59.5144	410	**-2.0**	0.2
Steenstrup Glacier North	27	75.36089	-57.8248	461	-5.5	-4.4	**-4.9**	75.35976	-57.8180	400	**-6.5**	0.2
Kangiata Nunaata Sermia	36	64.17541	-49.3341	1009	-2.0	-1.4	**-1.8**	64.17633	-49.3362	1000	**-1.7**	0.2
Kangerlussuup Sermersua[e]	47	71.46679	-51.1524	297	-0.9	3.0	**0.9**	71.46718	-51.1457	290	**-1.0**	0.2
Vestfjord Glacier	48	70.30724	-29.4261	770	-0.7	-0.5	**-0.6**	70.29696	-29.4331	780	**-0.4**	1.2
Zachariae Isstrøm	51	78.92388	-20.8077	120	-2.6	-2.4	**-2.5**	78.94335	-20.7679	90	**-4.3***	2.4
Mælkevejen[f]	73	63.65293	-41.7944	720	-9.5	-2.6	**-5.6**	63.65827	-41.7732	750	**-6.8**	1.1
Nioghalvfjerdsfjorden, 79North	74	79.21253	-25.2469	914	-0.3	-0.1	**-0.2**	79.21373	-25.2426	920	**-0.1**	0.2
Eqalorutsit Killiit Sermiat	76	61.36191	-46.4274	1152	-2.1	-1.1	**-1.4**	61.32520	-46.4221	1100	**-0.6**	4.0
Petermann Glacier	78	80.24614	-57.8308	874	-0.4	-0.2	**-0.3**	80.24422	-57.8319	800	**-0.3**	0.2
Hagen Bræ	111	81.33788	-29.0240	483	-10.0	-2.6	**-5.3**	81.35498	-29.0912	500	**-6.3**	2.2
Humboldt Glacier	139	79.80011	-64.1371	153	-2.4	-0.5	**-1.1**	79.64374	-63.8909	80	**-1.9**	18.0
Ryder Glacier	144	81.54270	-50.2471	135	-1.8	-1.0	**-1.4**	81.57002	-50.1459	110	**-2.3**	3.5
Steensby Glacier	159	81.12895	-53.8339	815	-0.9	-0.5	**-0.6**	81.12837	-53.8706	870	**-0.6**	0.65
Storstrømmen stagnant	225	76.76489	-22.9847	68	-3.2	-1.9	**-2.5**	76.78873	-22.9486	80	**-2.0**	2.8
Storstrømmen upstream	225	77.53578	-24.1847	864	0.9	1.2	**1.0**	77.56463	-23.8512	850	**2.0**	8.8
L. Bistrup Bræ stagnant	242	76.64136	-22.8025	131	-3.5	-2.9	**-3.2**	76.65332	-22.8105	130	**-2.6**	1.3
L. Bistrup Bræ upstream	242	76.32131	-23.1565	602	0.9	1.0	**1.0**	76.27288	-23.0847	630	**2.2***	5.8

[a] Glacier names and IDs are from ref. 24 and glacier names mentioned in this paper are shown in bold letters.

[b] Distance between locations of elevation change reconstructions from this study and from ref. 27.

[c] Surface elevation on August 31, 2006.

[d] Large difference between dh/dt reconstructions is marked by *.

[e] Large and rapid elevation changes, similar to surface signatures of subglacial lake drainage in Antarctica (10) or proglacial lake drainage on Daugaard-Jensen Glacier (ref. 26, Fig. S2*D*).

[f] labeled as Bernstorff South in ref. 27.

Table S4. Annual ice sheet volume loss rates between 1 September 2003 and 31 August 2009. All units are [$km^3 \cdot y^{-1}$]. Drainage basins are shown in Fig. 2*B*. Balance years are from September 1 to August 31.

NW	Total	SMB	Firn	Dyn.	N	Total	SMB	Firn	Dyn.	NE	Total	SMB	Firn	Dyn.
03-04	-15±4	32±10	-5±5	-42±12	03-04	-14±1	-14±4	1±1	-1±4	03-04	-21±1	-21±6	5±5	-5±8
04-05	-29±4	8±2	-5±5	-32±7	04-05	-2±1	-11±3	1±1	8± 4	04-05	5±1	-5±2	5±5	5±5
05-06	–61±4	-13±4	-5±5	-43±7	05-06	-1±1	-11±3	1±1	9±4	05-06	10±1	5±2	5±5	0±5
06-07	-81±4	-32±10	-5±5	-44±12	06-07	-8±1	-14±4	1±1	5±4	06-07	8±1	6±2	5±5	-3±5
07-08	-89±4	-47±14	-5±5	-37±15	07-08	-20±1	-21±6	1±1	0±6	07-08	-3±1	0±2	5±5	-8±5
08-09	–92±4	-43±13	-5±5	-44±14	08-09	-38±1	-25±8	1±1	-14±8	08-09	-21±1	-16±5	5±5	-10±7
Ave.	**-61±2**	**-16±4**	**-5±2**	**-40±5**	**Ave.**	**-14±1**	**-16±2**	**1±0**	**1±2**	**Ave.**	**-4±1**	**-5±1**	**5±2**	**-4±3**
Total	**-367±11**	**-95±24**	**-30±12**	**-242±29**	**Total**	**-83±3**	**-96±12**	**6±2**	**7±13**	**Total**	**-22±3**	**-31±9**	**30±12**	**-21±15**

Jak	Total	SMB	Firn	Dyn.	GrIS	Total	SMB	Firn	Dyn.	E	Total	SMB	Firn	Dyn.
03-04	-14±8	27±8	-5±5	-36±12	03-04	-197±17	40±15	-39±29	-198±37	03-04	-14±2	-2±1	-5±5	-7±5
04-05	-22±7	13±4	-5±5	-30±9	04-05	-321±16	-68±19	-39±29	-214±38	04-05	-23±2	-6±2	-5±5	-12±6
05-06	-34±7	2±1	-5±5	-31±9	05-06	-300±16	-141±29	-39±29	-120±44	05-06	-15±2	-7±2	-5±5	-3±6
06-07	-38±7	-6±2	-5±5	-27±9	06-07	-288±16	-180±32	-39±29	-69±46	06-07	-4±2	-5±2	-5±5	6±6
07-08	-39±7	-11±3	-5±5	-23±9	07-08	-282±16	-182±28	-39±29	-61±43	07-08	7±2	2±2	-5±5	10±6
08-09	-38±7	-13±4	-5±5	-20±9	08-09	-274±16	-137±23	-39±29	-98±40	08-09	20±2	4±1	-5±5	21±6
Ave.	**-31±3**	**2±2**	**-5±2**	**-28±4**	**Ave.**	**-277±7**	**-111±10**	**-39±12**	**-127±17**	**Ave.**	**-5±1**	**-2±1**	**-5±2**	**3±3**
Total	**-185±21**	**12±11**	**-30±12**	**-167±26**	**Total**	**-1662±42**	**-668±61**	**-234±71**	**-760±103**	**Total**	**-29±6**	**-14±4**	**-30±12**	**15±14**

SW	Total	SMB	Firn	Dyn.	SE	Total	SMB	Firn	Dyn.
03-04	28±8	8±2	-3±3	23±9	03-04	-147±12	10±3	-27±27	-130±30
04-05	16±7	-9±3	-3±3	28±8	04-05	-266±12	-58±17	-27±27	-181±34
05-06	-12±7	-24±7	-3±3	15±10	05-06	-187± 12	-93±28	-27±27	-67±41
06-07	-34±7	-36±11	-3±3	5±13	06-07	-131±12	-93±28	-27±27	-11±41
07-08	-50±7	-46±14	-3±3	-1±16	07-08	-88±12	-59±18	-27±27	-2±34
08-09	-56±7	-54±16	-3±3	-1±18	07-08	-49±12	10±3	-27±27	-32±30
Ave.	**-18±3**	**-27±4**	**-3±1**	**12±5**	**Ave.**	**-145±5**	**-47±8**	**-27±11**	**-71±14**
Total	**-108±18**	**-161±25**	**-18±7**	**71±32**	**Total**	**-868±29**	**-283±47**	**-162±66**	**-423±86**

Table S5. Annual ice sheet mass loss rates between 1 September 2003 and 31 August 2009. All units are [Gt $\cdot y^{-1}$]. Drainage basins are shown in Fig. 2*B*. Balance years are from September 1 to August 31.

NW	Total	SMB	Dynamics	N	Total	SMB	Dynamics	NE	Total	SMB	Dynamics
03-04	-31±11	8±2	-39±11	03-04	-14±6	-13±4	-1±4	03-04	-26±10	-21±6	-5±7
04-05	-33±7	-4±1	-29±6	04-05	-5±5	-12±4	7±3	04-05	-4±5	-9±3	5±5
05-06	-56±8	-17±5	-39±6	05-06	-5±5	-13±4	8±3	05-06	-5±5	-5±2	0±5
06-07	-67±14	-27±8	-40±11	06-07	-10±6	-15±5	5±4	06-07	-7±5	-4±1	-3±5
07-08	-70±17	-36±11	-34±14	07-08	-19±8	-19±6	0±6	07-08	-13±5	-6±2	-7±5
08-09	-83±18	-43±13	-40±13	08-09	-37±10	-24±7	-13±7	08-09	-25±8	-16±5	-9±6
Ave.	**-57±6**	**-20±3**	**-37±5**	**Ave.**	**-15±3**	**-16±2**	**1±2**	**Ave.**	**-13±3**	**-10±1**	**-3±2**
Total	**-341±33**	**-119±20**	**-222±27**	**Total**	**-90±17**	**-96±12**	**6±12**	**Total**	**-80±16**	**-61±9**	**-19±13**

Jak	Total	SMB	Dynamics	GrIS	Total	SMB	Dynamics	E	Total	SMB	Dynamics
03-04	-25±11	8±2	-33±11	03-04	-209±35	-27±8	-182±34	03-04	-11±5	-5±2	-6±5
04-05	-27±8	1±1	-28±8	04-05	-293±38	-97±17	-196±35	04-05	-19±6	-8±2	-11±6
05-06	-33±8	-4±1	-29±8	05-06	-258±48	-147±25	-111±41	05-06	-12±6	-9±3	-3±6
06-07	-33±9	-8±2	-25±8	06-07	-232±50	-169±27	-63±43	06-07	0±6	-6±2	6±6
07-08	-33±9	-12±4	-21±8	07-08	-238±47	-182±26	-56±39	07-08	6±6	-3±1	9±6
08-09	-31±9	-13±4	-18±8	08-09	-231±43	-141±21	-90±39	08-09	22±7	3±1	19±6
Ave.	**-30±4**	**-5±1**	**-26±4**	**Ave.**	**-243±18**	**-127±9**	**-116±16**	**Ave.**	**-2±2**	**-5±1**	**2±2**
Total	**-182±24**	**-28±6**	**-154±24**	**Total**	**-1460±106**	**-763±53**	**-698±94**	**Total**	**-14±14**	**-28±4**	**14±14**

SW	Total	SMB	Dynamics	SE	Total	SMB	Dynamics
03-04	21±8	-0±1	21±8	03-04	-123±28	-4±1	-119±28
04-05	12±8	-14±4	26±7	04-05	-217±35	-51±15	-166±31
05-06	-10±12	-24±7	14±9	05-06	-136±44	-75±25	-61±38
06-07	-28±15	-33±10	5±12	06-07	-86±44	-76±23	-10±38
07-08	-42±19	-41±12	-1±15	07-08	-67±37	-65±20	-2±31
08-09	-46±22	-47±14	1±17	08-09	-30±28	-1±1	-29±28
Ave.	**-16±6**	**-27±4**	**11±5**	**Ave.**	**-110±15**	**-45±7**	**-65±13**
Total	**-94±37**	**-159±23**	**65±29**	**Total**	**-630±89**	**-272±41**	**-388±79**

Table S6. Comparison of total GrIS and regional mass balance estimates (in Gt $\cdot y^{-1}$) from this study with previous results. LAS: laser altimetry, GRACE: Gravity Recovery and Climate Experiment (GRACE) satellite gravimetry, IOM: input-output method.

Publication	Method	Time Span	Region[a]	Total mass balance (Gt $\cdot y^{-1}$)[b]		Dynamic	SMB
				Publication	This study	(Gt $\cdot y^{-1}$)	(Gt $\cdot y^{-1}$)
This study	LAS	2003/09/01-2009/08/31	GrIS		-243±18	-116±16	-127±9
This study	LAS	2003/09/01-2008/08/31	GrIS		-246±20	-122±18	-124±11
This study	LAS	2003/09/01-2007/08/31	GrIS		-248±23	-138±19	-110±10
This study	LAS	2005/09/01-2009/08/31	GrIS		-240±22	-80±20	-160±13
Sørensen et al., 2011 (19)	LAS	Oct 2003 - Mar 2008	GrIS	**191±23** to -240±28	-246±20 -246±20		
Zwally et al., 2011 (28)	LAS	2003-2007	GrIS	**-171±4**	-248±23		
Shepherd et al., 2012 (29)	LAS	2003/10/01-2008/10/01	GrIS	**-185±24**	-246±20		
Sasgen et al., 2012 (30)	LAS	Oct 2003 - Oct 2009	GrIS	-245±28	-243±18		
Khan et al., 2014 (31)	LAS	Apr 2003 - Apr 2009	GrIS	-232±32	-243±18	-135±39	-97±23
Shepherd et al., 2012 (29)	GRACE	2003/10/01-2008/10/01	GrIS	-228±30	-246±20		
Sasgen et al., 2012 (30)	GRACE	Oct 2003 - Oct 2009	GrIS	-230±29	-243±18		
Khan et al., 2014 (31)	GRACE	Apr 2003 - Apr 2009	GrIS	-231±30	-243±18		
Chen et al., 2011 (32)	GRACE	Apr 2002 - Nov 2009	GrIS	-219±38	-243±18		
Luthcke et al., 2013 (33)	GRACE	2003/12/01-2010/12/01	GrIS	-230±12	-243±18		
Shepherd et al., 2012 (29)	IOM	2003/10/01-2008/10/01	GrIS	-284±65	-246±20		
Sasgen et al., 2012 (30)	IOM	Oct 2003 - Oct 2009	GrIS	-260±53	-243±18		
Enderlin et al., 2014 (34)	IOM	2005-2009	GrIS	-265±18	-240±22	-95	-170
Rignot et al., 2011 (35)	IOM	Nov 2002 - Jun 2009	GrIS	-250±40	-243±18		
van Broeke et al., 2009 (36)	IOM	2003/01/01-2008/12/31	GrIS	-237±20	-246±20	-94	-144
Kjeldsen et al., 2013 (37)	LAS	2005-2009	NW	-59 ±9	-69±7		
Sasgen et al., 2012 (30)	LAS	Oct 2003 - Oct 2009	C, D, E/*E, SE*	-109±22	-112±18		
Sasgen et al., 2012 (30)	LAS	Oct 2003 - Oct 2009	B/*NE*	-16±3	-13±3		
Sasgen et al., 2012 (30)	LAS	Oct 2003 - Oct 2009	A/*N*	-16±1	-15±3		
Sasgen et al., 2012 (30)	LAS	Oct 2003 - Oct 2009	G/*NW*	-53±3	-57±7		
Sasgen et al., 2012 (30)	LAS	Oct 2003 - Oct 2009	F/*SW, Jak*	-51±7	-46±8		
Chen et al., 2011 (32)	GRACE	Apr 2002 - Nov 2009	1, 2, 3/*SE*	-101	-110±18		
Chen et al., 2011 (32)	GRACE	Apr 2002 - Nov 2009	4/*E*	-9	-2±3		
Chen et al., 2011 (32)	GRACE	Apr 2002 - Nov 2009	5, 6/*NE*	-18	-13±3		
Chen et al., 2011 (32)	GRACE	Apr 2002 - Nov 2009	7, 8/*N*	-8	-15±3		
Chen et al., 2011 (32)	GRACE	Apr 2002 - Nov 2009	9, 10/*NW*	-46	-57±7		
Chen et al., 2011 (32)	GRACE	Apr 2002 - Nov 2009	11/*Jak*	-30	-30±4		
Chen et al., 2011 (32)	GRACE	Apr 2002 - Nov 2009	12/*SW*	-10	-16±7		

[a] Region names in refs. 30 and 32 are shown according to the original publications (left) and to this study (right, in italic).
[b] Bold letters mark a large difference compared to this study.